

Cosmic Rays, CFCs, Ozone Hole and Global Climate Change: Understandings from a Physicist

Q.-B. Lu

*Department of Physics and Astronomy and Departments of Biology and Chemistry, University
of Waterloo, Waterloo, Ontario, CANADA*

Abstract This paper reviews comprehensive observed data and uses simple physical models with few parameters to evaluate the underlying mechanisms for the ozone hole and recent global climate changes. The cosmic-ray-driven electron-induced-reaction (CRE) mechanism and the greenhouse effect of CFCs are first reviewed briefly. It is followed by statistical analyses of comprehensive measured datasets of quantities, including cosmic rays (CRs), total solar irradiance, sunspot number, halocarbons (CFCs, CCl₄ and HCFCs), CO₂, total O₃, lower stratospheric temperatures and global surface temperatures, to examine natural and anthropogenic contributions to O₃ loss and global climate change. For O₃ depletion, new statistical analyses of the CRE equation with observed total O₃ and stratospheric temperature data give high linear correlation coefficients ≥ 0.92 . After the removal of the CR effect, *a pronounced recovery by 20~25% of the Antarctic O₃ hole is found, while no recovery of O₃ loss in mid-latitudes has been observed.* This is consistent with the CRE mechanism. For global climate change, detailed analyses of time-series data of multiple physical quantities clearly show that the natural (solar/CR) factor has played a negligible effect on Earth's climate since 1970. *Remarkably, statistical analyses of observed data give a linear correlation coefficient as high as 0.98 between global surface temperatures and total amounts of stratospheric halocarbons in 1970-2011.* Furthermore, a refined recalculation of the greenhouse effect of halocarbons shows that *they (mainly CFCs) could alone result in the global surface temperature rise of ~0.6 °C in 1970-2002.* These results demonstrate that the recent global warming was mainly caused by the greenhouse effect of anthropogenic halocarbons rather than CO₂. Thus, a slow reversal of global temperature to the 1950 value is expected for coming 5~7 decades.

Keywords: Cosmic rays, CFCs, Solar variability, Ozone hole, Global warming, Global cooling

PACS: 34.70.+e, 34.80.Ht, 34.35.+a, 73.20.At, 82.30.Fi, 82.65.+r, 94.20.Wq, 92.60.Ry

I. Introduction

There is long and strong interest in studies of halogen-containing molecules; one of the major characteristics is their extremely strong oxidizing capability, i.e., high reactivity with an electron.¹⁻³ Electron-transfer reactions play important roles in many processes in physics, chemistry, atmosphere, environment, biology and medicine.¹⁻⁸ For instance, dissociative electron transfer (DET) reactions of molecules with weakly-bound, ultrashort-lived prehydrated electrons play key roles in many environmental and biological processes, ranging from the formation of the ozone hole^{7,9-12} to DNA strand breaks^{8,13,14}. In particular, DET is an extremely effective process for reactions of halogenated molecules, such as chlorofluorocarbons (CFCs), halopyrimidines and cisplatin, with prehydrated electrons trapped on solid ice surfaces^{9-11,15-27} and in liquid water²⁸⁻³⁴, which have implications for atmospheric ozone depletion and the activation of anticancer drugs for radiotherapy of cancer, respectively. Furthermore, it was recently found that atmospheric CFCs as greenhouse gases may also play the major role in recent global warming observed in the late half of the 20th century.^{35,36} Since ozone depletion and global warming are two major scientific problems of global concern, further investigation of physical and chemical processes of halogenated molecules and their effects on the Earth climate and environment may have great significance.

Both natural and anthropogenic impacts may alter the Earth's climate and environment. First, there is long interest in studying the effects of natural factors such as solar activity and cosmic rays (CRs) on the Earth's ozone layer.³⁷⁻⁴⁶ However, it has been shown that pure natural effects play a limited role in forming the O₃ hole observed since the 1980s.⁷ Thus, they will not be further discussed in this study; one of the focuses will be on the significant and long-term (inter-annual) variation of the O₃ hole.

Second, with global warming observed in the late half of the 20th century, the debate on the extent to which the Sun affects the Earth's climate has become intense.⁴⁷⁻⁵⁷ For example, a number of studies showed good correlations between solar activity and the temperature of the Earth's atmosphere on wide-range time scales of decades to centuries.⁴⁹⁻⁵³ Three main mechanisms for centennial-scale solar effects on climate have been proposed.^{54,57} These include changes in the energy input into the Earth's atmosphere through variations in total solar irradiance (TSI), changes in stratospheric chemistry through variations of solar UV irradiance and changes in cloud cover induced by the CR flux, which is modulated by the strength of the Sun's magnetic field. For the latter, there is considerable interest in studying the role of ions produced by CRs in the formation of aerosols and clouds in the troposphere⁵⁸⁻⁶⁰ and in the polar stratosphere^{61,62}. However, the exact role of CRs in Earth *surface* climate variations is unclear. In fact, there have been indications that the variation of solar quantities cannot explain the

drastic global surface temperature rise (~ 0.6 °C) in the late half of the last century.⁵⁴⁻⁵⁷ These controversies have centred on the solar influence of climate over the past three solar cycles.

Third, severe ozone depletion is known to be associated with man-made CFCs such as CF_2Cl_2 (CFC-12) and CFCl_3 (CFC-11) and the conventional understanding is the photodissociation mechanism.⁶³⁻⁶⁷ Since its first surprising observation in 1985,⁶⁸ the large Antarctic ozone hole appears in the lower polar stratosphere in every early springtime. The Montreal Protocol has successfully phased out the world-wide production and use of CFCs, and as a result, the observed total halogen in the lower atmosphere has been declining since ~ 1994 . This should have led to clear recoveries in ozone loss, even with delays of ~ 3 and ~ 6 years in equivalent effective stratospheric chlorine levels at mid-latitudes and Antarctica from the tropospheric peak.^{65,66} However, no statistically significant recovery of ozone loss in either mid-latitudes or the polar region has directly been observed.⁶⁷ Even in more obvious contrast to the predictions from photochemical models, the O_3 loss is anti-phased with the solar activity, that is, O_3 loss maxima (minima) correspond to solar activity minima (maxima), e.g., in 1987, 1998 and 2008 (1991 and 2002), as shown in Figure 1. These observed results indicate that the current photochemical theory of O_3 loss is incomplete and very limited. In fact, current atmospheric chemistry-climate models have difficulties to predict the future polar O_3 loss, and improving the predictive capabilities is one of the greatest challenges in polar ozone research.⁶⁹

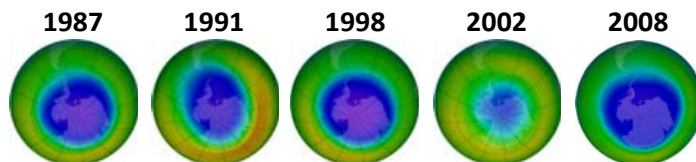
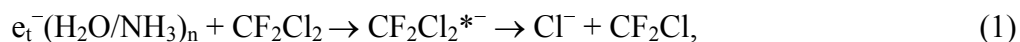


Figure 1. Eleven-year cyclic Antarctic ozone holes (satellite images credited to NASA).

Fourth, there is particularly a long history of studies of dissociative attachment (DA) of CFCs to low-energy free electrons since the 1950s.⁷⁰⁻⁷⁵ The DA process was long thought to be unimportant for CFCs in the stratosphere because most of the free electrons are captured by more abundant O_2 .^{76,77} However, this understanding has changed since the surprising finding by Lu and Madey^{9,10} that the Cl^- yield in electron-stimulated desorption (ESD) of CFCs was enhanced by *up to 30000 times* when CFCs were adsorbed on polar $\text{H}_2\text{O}/\text{NH}_3$ ice surfaces. In the latter experiments, electron-induced dissociation cross sections of CFCs were measured to be up to $6 \times 10^{-12} \text{ cm}^2$, which is 10^8 times the photodissociation cross sections (10^{-20} cm^2) of gaseous CFCs. Moreover, a dissociative electron transfer (DET) mechanism was also proposed to explain the observed Cl^- yield enhancements:



where e_t^- is a weakly-bound electron trapped in the polar ($\text{H}_2\text{O}/\text{NH}_3$) ice.^{9,10} In contrast to the DA process of free electrons, no kinetic energy is involved in the DET reaction. This finding has stimulated significant interest in studying electron-induced reactions of CFCs in polar media, as evidenced by observations in ESD experiments^{9,10,15-17}, electron trapping experiments¹⁸⁻²⁰ and femtosecond time-resolved laser spectroscopic measurements in polar liquids^{28,29,32,33} or on ice surfaces^{21,24,26}. Interestingly, the very large DET cross section up to $4 \times 10^{-12} \text{ cm}^2$ for CFCl_3 on D_2O ice, measured most recently by Stähler et al.²⁶, is comparable to the values of $\sim 1 \times 10^{-14}$ and $\sim 6 \times 10^{-12} \text{ cm}^2$ for CF_2Cl_2 adsorbed on H_2O and NH_3 ice respectively, originally measured by Lu and Madey⁹. Several theoretical studies have also confirmed the DET mechanism.^{23,25,27} It is now a very well established fact that electron-induced dissociations of organic and inorganic chlorine, bromine and iodine containing molecules such as CFCs and HCl (ClONO_2) by the presence of polar media in various phases can be greatly enhanced via the DET mechanism.^{7,26}

Lu and Madey⁹ also proposed that halogen anions (Cl^-) from DET reactions of halogenated molecules can be converted into active halogens to destroy ozone and this DET process should be considered as an unrecognized mechanism for the formation of the O_3 hole. And Lu and Sanche^{11,12} have subsequently searched the impact of DET reactions of halogenated molecules on the O_3 layer. In the stratosphere, electrons are mainly produced via atmospheric ionization by cosmic rays (CRs). The CR-driven electron-induced reaction (CRE) mechanism, as schematically shown in Fig. 2, has been proposed as an important mechanism for the formation of the O_3 hole.^{7,9,11,12} As reviewed recently,⁷ numerous data from field measurements have provided strong evidence of the CRE mechanism.

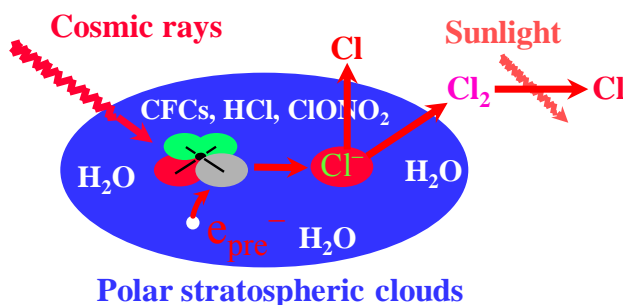


Figure 2. The CRE mechanism^{7,9,11,12}: Cosmic-ray driven electron-induced reactions of halogen-containing molecules in polar stratospheric clouds (PSCs) result in the formation of Cl^- ions, which can either be rapidly converted to reactive Cl atoms to destroy ozone or react with other species to release photoactive Cl_2 and ClONO_2 in the winter polar stratosphere. The latter species can also then produce Cl atoms to destroy O_3 , upon photolysis in the spring polar stratosphere.

Fifth, apart from their well-known role in ozone depletion, CFCs are also long-known greenhouse (GH) gases.^{66,67,78-84} In 1975, Ramanathan⁷⁸ made the first calculations that the GH effect by CFCs and chlorocarbons could lead to a rise of $\sim 0.9 \text{ K}$ in global surface temperature if each atmospheric

concentration of these compounds was increased to 2 parts per billion (ppb). However, the actual atmospheric concentrations of halocarbons have been observed to be far less than 2 ppb due to the successful regulation by the Montreal Protocol. It has been generally thought that halocarbons would play a certain but not dominant role in surface temperature changes, compared with the GH effect of non-halogenated gases (CO_2 , CH_4 and N_2O).^{79,82} Since the current CO_2 concentration, >390 parts per million (ppm), is *six orders of magnitude* higher than those of halocarbons in ppt, current climate models give that the total radiative forcing ΔF of halocarbons represents only ~17% of the calculated ΔF (~1.7 W/m²) of CO_2 .^{83,84,66,67} It was thus concluded that CO_2 would play the dominant role in recent global warming.

However, it should be noted that in climate models mentioned above, no saturation in GH effect of non-halogenated molecules was assumed. In striking contrast, recent findings have strongly indicated that this assumption is invalid,^{7,35,36} and the actual role of halocarbons in global climate change was re-evaluated.³⁵ The latter has shown that the increase of atmospheric halocarbons (mainly CFCs) is likely to cause the observed global surface temperature rise of 0.5~0.6 °C from 1950 to 2002 and global temperature is expect to reverse slowly with the projected decrease of CFCs in coming decades. This conclusion seems to be very surprising, but it is consistent with the 2011 WMO Report.⁶⁷ The latter states that “*There have been no significant long-term trends in global-mean lower stratospheric temperatures since about 1995*”, and that following an apparent increase from 1980–2000, the stratospheric water vapor amount has decreased in the past decade. These observations are “not well understood” from photochemistry-climate models,⁶⁷ but are consistent with the observed global temperature recovery.^{7,35} Most recently, Revadekar and Patil³⁶ have also found the positive correlation between surface temperature and CFCs over the region of India.

The purpose of this study is to make an *objective presentation* of comprehensive observed data and *statistical analyses* of the data based on simple physical models with few parameters. First, brief reviews on the CRE mechanism of the O_3 hole and the CFC mechanism of global warming will be given in Sections II and III, respectively. Subsequently, comprehensive time-series datasets of CRs, atmospheric equivalent effective chlorine (EECl), total ozone, lower polar stratospheric temperatures and global surface temperatures will be presented in Sections IV. The natural (CR) effect will be taken out from observed data of total O_3 to reveal the actual effect of man-made CFCs on O_3 loss, and the conclusion will be examined by *statistical correlation analyses* of the CRE mechanism with observed time-series data of halocarbons, CRs, O_3 loss and stratospheric cooling over Antarctica. This should give a more true evaluation of the effectiveness of the Montreal Protocol. In Section V, the future trend of the Antarctic O_3 hole will be predicted from these analyses. Furthermore, to evaluate the natural and

human effects on Earth's surface temperature since 1850, substantial time series datasets of CO₂, halocarbons as well as the most relevant solar activity indicators including total solar irradiance (TSI), sunspot number (SSN) and CR intensity from multiple independent sources will be examined in detail in Sections VI and VII. Time series TSI data will include reconstructions based on models and proxies in pre-1976 and constructions based on direct measurements available since 1976. Particularly, CR measurements from as many as *ten independent stations* in different locations from the polar region to mid- and low-latitudes will be presented. Based on observed facts, a refined re-evaluation of the GH effect of halocarbons will be presented in VIII. Quantitative analyses will be emphasized on the influences of humans and the Sun on global surface temperature since 1970 for several reasons. First, there is much less controversy about the solar effect on the Earth's climate for the pre-1970s. Second, the significant rise in global surface temperature occurred from 1970 to around 2000. Third, direct measurements of TSI and CFCs have only been available since the 1970s when considerable atmospheric impact (O₃ loss) of CFCs started to be observed. Thus, the significant anthropogenic effect on Earth's climate is expected to begin around 1970, and reliable conclusions are achievable. Moreover, the future trend of global surface temperature will be presented in Section IX and future changes of global sea level will be discussed in Section X. Finally, the conclusions will be given in Section XI. *These observations and analyses aim to improve our fundamental understandings of the polar O₃ hole and global climate change and enhance our predictive capabilities.*

II. The Cosmic-Ray-Driven Theory of the Ozone Hole

As outlined below, the CRE mechanism has several features distinguishing from photochemical models of ozone depletion.

(1) The CRE mechanism has strong *latitude* and *altitude* effects corresponding to the distribution of electrons produced by CRs in the atmosphere. Since CRs are composed of charged particles, the earth's magnetic field focuses them onto the South and North Poles, and due to atmospheric ionization, the electron production rate has a maximum at ~18 km above the ground. On the other hand, on top of the general stratosphere, the detected free electron concentration drops sharply with descending altitudes: it is ~10³ electrons cm⁻³ at ~85 km, and ~10 electrons cm⁻³ at 60 km.^{76,77} Below this height, the free electron density is too low to detect, as most free electrons are captured by atmospheric molecules (mainly O₂). Consequently, electron-induced decompositions of halogen-containing gases take place mainly in the upper general stratosphere at high latitudes. But the situation is drastically different in the lower polar stratosphere in winter due to the presence of PSCs.⁹⁻¹² Electrons produced by CRs can effectively be trapped in PSC ice and transferred to adsorbed halogenated molecules. As

shown in Fig. 3A-D, strong *spatial* correlations between CR intensity, CFC dissociation and ozone loss in the Earth's atmosphere with variations of latitude and altitude have been well observed.^{7,11,85} Ozone loss occurs mainly in the polar stratosphere (Fig. 3A), and the O₃ hole is exactly located at the polar stratosphere at 15~18 km (Fig. 3B). Also shown in Fig. 3B is the observed O₃ loss over northern mid-latitudes (40°-53°N) from 1979 to 1998: apart from the expected O₃ loss maximum at ~40 km, there is also an O₃ loss peak in the lower stratosphere at the altitude of ~15 km.

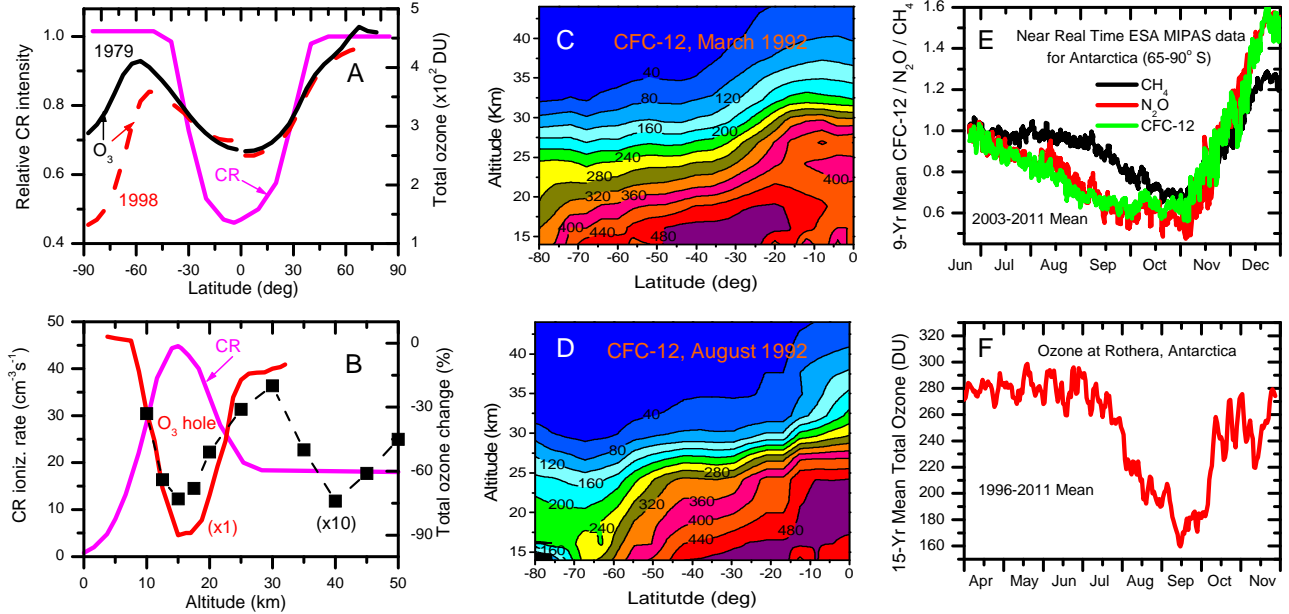


Figure 3. Spatial and time correlations between cosmic-ray (CR) intensity, CFC dissociation and ozone depletion. A: Latitude dependences of CR intensity and monthly mean total ozone in pre-O₃ hole (Oct. 1979 for Antarctica and March 1979 for Arctic) and O₃ hole period (dashed line for Oct. 1998 for Antarctica and March 1998 for Arctic); B: Altitude dependences of the springtime O₃ hole over Syowa, Antarctica (the red line) and O₃ loss per decade from 1979 to 1998 over northern midlatitudes (40°-53°N) (the squares).¹¹ C and D: 27-31 March (fall) and 16-23 August (winter) 1992 CF₂Cl₂ levels in ppt from NASA UARS's CLEAS datasets.⁷ E: 9-year mean time-series data of CFC-12, N₂O, CH₄ are averaged from the ESA's MIPAS Near Real Time (daily) satellite data in the lower Antarctic stratosphere (65-90° S) during winter months (June 23-September 30) in 2003-2011, where the data for each gas were normalized to its initial value in the beginning of winter.⁸⁵ F: The 15-year mean time series total O₃ data are averaged from "Real-time" daily total O₃ data at Rothera in Antarctica over the past 16 years (1996-2011) recorded by the British Antarctic Survey (BAS).⁸⁵ In E and F, the 2002 data were not included due to the unusual split of the polar vortex in 2002.⁶⁶

The concentration distribution of CFCs is generally anti-correlated with the CR intensity distribution, and the decomposition of CFCs is drastically enhanced in the lower polar stratosphere during winter (Fig. 3C and D). Time-series data of CH₄ and CFC-12 from the NASA UARS satellite datasets during the winter season were reported earlier,⁷ showing significant depletion of CFCs but not CH₄ in the winter months. More recently, a similar result was also observed from ESA's MIPAS Near Real Time daily satellite data of CFC-12, N₂O and CH₄ in the lower Antarctic stratosphere (65-90° S) during the winter season (June 23-September 30) over the past ten years (2002-2011).⁸⁵ The 9-year (2003-2011) mean time-series data are shown in Fig. 3E, which indeed shows that the CFC-12 data exhibit a

variation curve that overlaps well with that of the N₂O data, while the CH₄ data show a very different curve. It is clearly confirmed that the CFC-12 and N₂O levels exhibit a similar continuous decrease since the beginning of winter, while the CH₄ level does not decrease until the end of August. After that, all gases show decreasing trends in September-October and then rising trends in November. Note that in September and October, the levels of all gases (CH₄, N₂O and CFC-12) drop in the polar lower stratosphere. This can be well explained by significant stratospheric cooling and air descending as a result of severe O₃ loss in the springtime lower polar stratosphere. These data have provided strong evidence of CRE (DET) reactions of CFCs and N₂O but not CH₄ in the *winter* polar stratosphere.

The CRE mechanism can lead to the formation of reactive halogen species to destroy ozone in both the *winter* polar stratosphere in the dark and the *springtime* polar stratosphere with sunlight.^{7,9} The British Antarctic Survey (BAS)'s real-time daily total O₃ variations at Rothera, Antarctica over the whole years since 1996 were also shown recently.⁸⁵ The 15-year mean time series total O₃ data are shown in Fig. 3F, which clearly shows that total O₃ starts to drop from a high value of about 300 DU at the beginning of July to about 220 DU at the middle of August and to a minimum value as low as 150 DU in September. Note that due to the lack of sunlight in the lower polar stratosphere during early and mid-winter, the significant polar O₃ loss in July and early August cannot be explained by photochemical models. The real-time variation of total O₃ (Fig. 3F) generally follows well that of CFCs or N₂O (Fig. 3E) during the winter season, indicating that the CRE mechanism plays an important role in causing severe O₃ loss over Antarctica.

(2) The CRE model has predicted an *~11-year cyclic* variation of O₃ loss in the polar hole corresponding to the solar cyclic variation of the CR intensity that has an average periodicity of 11 years (varying in 9-14 years).^{7,11,12} One should recall that because the oscillation amplitude of the CR intensity in 11-year CR cycles is well-known to be small, only about 10% of its mean value, the oscillation amplitude of polar stratospheric ozone would be too small to observe if the CRE mechanism played only a minor role. In contrast, high-quality ozone data from NASA satellites have shown a pronounced *~11-year cyclic* correlation between CR intensity and 3-month average total O₃ data in the O₃ hole period over Antarctica (60-90° S).⁷ Moreover, it is also well-known that O₃ loss can cause a stratospheric cooling: less O₃ in the stratosphere implies less absorption of solar and infra-red radiation there and hence a cooler stratosphere. Thus, temperature data in the lower polar stratosphere is a direct indicator of polar O₃ loss. Indeed, a clear 11-year cyclic correlation between CR intensities and lower stratospheric temperatures at the Antarctic Halley station (75°35'S, 26°36'W) in November following the O₃ hole peak over the past 50 years (1956-2008) has also been found.⁷

(3) A simple quantitative expression of ozone loss due to the CRE mechanism has been found, in which total ozone loss ($\Delta[O_3]_i$) in the polar stratosphere is given by:⁷

$$\frac{\Delta[O_3]_i}{[O_3]_0} = \frac{[O_3]_i - [O_3]_0}{[O_3]_0} = -k \times [C_i] \times I_i \times I_{i-1}, \quad (2)$$

where $[C_i]$ the equivalent effective chlorine (EECl) in the polar stratosphere, $\Delta[O_3]_i/[O_3]_0$ is the relative total O_3 change, $[O_3]_0$ the total O_3 in the polar stratosphere when $[C_i]=0$, I_i and I_{i-1} the CR intensities in the current and preceding years respectively, and k a constant. In Eq. 2, two effects of CRs are implied: the formation of reactive halogens from CRE reactions in PSCs should be linearly proportional to I_i and $[C_i]$; both CR-produced ions and O_3 -loss-induced stratospheric cooling can affect the formation of PSCs.^{7,61,62} The latter effect may be delayed by ~ 1 year.⁷ It has been shown that Eq. 2 can reproduce well the observed 11-year cyclic variations of not only total O_3 but also stratospheric cooling over Antarctica in the past five decades.⁷ Immediately, Eq. 2 gives O_3 -loss maxima in 1987, 1998 and 2008 and minima in 1991 and 2002, in agreement with observed data (Fig. 1). More quantitative and statistical analyses of observed data in terms of Eq. 2 will be given in Section IV.

III. The CFC Theory of Global Warming

The explanation of blackbody radiation via the revolutionary concept of *energy quanta* put forward by Max Planck in 1900 is generally regarded as the dawn of 20th century quantum theory. Radiation from Earth's surface (after absorbing solar radiation) can approximately be treated as blackbody radiation. The radiation power in wavelength interval $d\lambda$ or frequency interval $d\nu$ is given by the Planck formula:

$$B_\lambda(T)d\lambda = \frac{8\pi hcV}{\lambda^5 (e^{hc/\lambda kT} - 1)} d\lambda, \quad \text{or} \quad B_\nu(T)d\nu = \frac{8\pi h V \nu^3}{c^3 (e^{h\nu/kT} - 1)} d\nu, \quad (3)$$

where $B_\lambda(T)$ is the power density per unit wavelength λ and $B_\nu(T)$ is the power density per unit frequency ν ($=c/\lambda$) at the temperature T , where k is Boltzmann's constant and h is Planck's constant. Power density is defined as the radiation intensity I , that is, the radiation energy per unit time per unit area. Traditionally, the wavelength λ_{\max} for the $B_\lambda(T)$ maximum is given by Wien's displacement law: $\lambda_{\max}=2898 \mu\text{m}\cdot\text{K}/T$. Since the mean Earth's surface temperature is ~ 285 K, $B_\lambda(T)$ will peak at

$\lambda_{\text{max}}=10.2 \text{ }\mu\text{m}$ in the infra-red (IR) wavelength range. Alternatively, $B_\nu(T)$ peaks at a wavenumber around 558.9 cm^{-1} , corresponding to $\lambda=17.9 \text{ }\mu\text{m}$.

Climate researchers often argued that the IR absorption band of CO_2 , which is at $600\text{-}770 \text{ cm}^{-1}$ ($\lambda=13\text{-}17 \text{ }\mu\text{m}$), would center at the blackbody radiation of the Earth. However, this is actually a misconception: neither $B_\lambda(T)$ nor $B_\nu(T)$ can be compared with the atmospheric absorption (transmittance) spectrum, since they are different in physical nature and units. This paradox can be solved with the integral of either $B_\lambda(T)$ over λ or $B_\nu(T)$ over ν , which must give the same intensity I .³⁵ Here, the space radiation intensity spectrum $I(\lambda)$ of the Earth surface at $T=285 \text{ K}$ in $\lambda=4\text{-}17 \text{ }\mu\text{m}$, together with a theoretical atmospheric transmittance spectrum, is shown in Figure 4, which gives an intensity peak around $10 \text{ }\mu\text{m}$. There are two reasons to call the spectral region of $\lambda=8\text{-}12 \text{ }\mu\text{m}$ as the atmospheric “window”. First, the unpolluted atmosphere is quite transparent in this spectral region, except for absorption by ozone at $9.6 \text{ }\mu\text{m}$; this is generally agreed by climate researchers. Second, another more critical reason is that the majority of Earth’s radiation energy is emitted into space at $\lambda=8\text{-}12 \text{ }\mu\text{m}$, where the maximum intensity of Earth’s blackbody radiation is located.

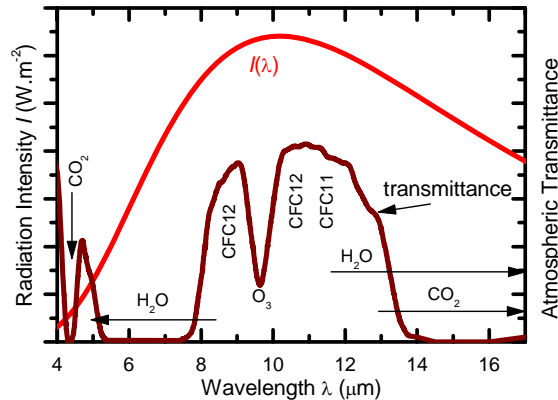


Figure 4. Blackbody radiation intensity spectrum $I(\lambda)$ and atmospheric transmittance spectrum of the Earth.³⁵

It follows that over 80% of the total radiation energy from Earth’s surface and clouds is emitted into space in the λ region of $8\text{-}12 \text{ }\mu\text{m}$. Therefore, any pollutant that strongly absorbs radiation at $\lambda= 8\text{-}12 \text{ }\mu\text{m}$ is a highly effective GH gas. Unfortunately, many halogen-containing molecules such as CFCs are not only major ozone-depleting molecules but also highly effective GH gases because of their strong absorption bands at $\lambda=8\text{-}12 \text{ }\mu\text{m}$.^{35,78,80}

As also shown in Figure 4, CO_2 contributes to strong absorption bands at $\lambda=4\text{-}5 \text{ }\mu\text{m}$ and $13\text{-}17 \text{ }\mu\text{m}$, while H_2O (water) is the most effective absorber in the entire IR spectral range with two major bands at $5\text{-}8.3 \text{ }\mu\text{m}$ and $11\text{-}17 \text{ }\mu\text{m}$. Thus, the key question is the relative importance of the GH effect of CFCs, to those of non-CFC gases (particularly CO_2). It is worthwhile to note that CO_2 , CH_4 and N_2O have high

atmospheric concentrations in 392 ppm, 1.9 ppm and 327 ppb, respectively, which are 10^6 , 10^4 and 10^3 times those of CFCs and HCFCs in 100-500 ppt.^{66,67} Although the CH₄ and N₂O levels are lower than CO₂, IR absorption band strengths of CH₄ at 7.6 μm and N₂O at 7.8 μm are 1~2 orders of magnitudes higher than that of CO₂ at 15 μm .^{79,80} Therefore, the absorption of the Earth IR radiation by these non-halogen gases is most likely to have saturated.

Indeed, the saturation in GH effect of non-halogen gases has indeed been observed in recent studies. For example, no signs of CO₂ warming effect on polar ozone loss and stratospheric temperature over Antarctica since the 1950s were recently found, and global warming from 1950 to 2000 was most likely caused by the human emission of CFCs into the atmosphere.⁷ Furthermore, changes in the Earth's GH effect can be detected from variations in the radiance spectrum of outgoing longwave radiation (OLR) at outer space, which is a measure of how the Earth radiation emits to space and carries the signature of GH gases that cause the warming effect. As first observed in a careful analysis of satellite data by Anderson et al.⁸⁶ and recently revisited by Lu³⁵, there exists the striking contrast between observed and CO₂-warming-theory predicted radiance difference between OLR spectra measured in 1970 and 1997 (spanning over the rapidest warming period). Indeed, the expected strong CO₂ absorption band in the 600 to 800 cm^{-1} region is *absent* in the observed difference spectrum. Moreover, detailed analyses by Fischer et al.⁸⁷ of high-resolution records from Antarctic ice cores showed that the CO₂ concentration increase by 80~100 ppm had a lag of 600~1000 years *after* the warming of the last three deglaciations, and despite strongly decreasing temperatures by about 5 °C, high CO₂ concentrations remained constant for thousands of years during glaciations. The results have questioned the application of the past CO₂-climate relation to the recent anthropogenic warming.⁸⁷ Further evidence of the saturated GH effect of non-halogen gases and the dominant role of halocarbons in altering the Earth climate since 1970 will be shown in Section VII.

IV. Evaluation of the Montreal Protocol

The observations mentioned above have shown that both total O₃ loss and stratospheric cooling in Antarctica can be well reproduced by Eq. 2 that leads to the dependence of O₃ loss on the EECl level [C_i] and CR intensity I_i only. The CR intensities have been well recorded since 1960s, showing a rising trend in the past four solar cycles.⁷ This means that no sign in recovery of recorded Antarctic O₃ losses is most likely due to rising CR intensities, which compensates the declining EECl levels in the polar stratosphere. Thus, the *real* change of the stratospheric EECl levels can be determined by correcting measured total O₃ data or temperature data in the lower polar stratosphere with the CR-factor of $1/(I_i I_{i-1})$.

1). Therefore the real effectiveness of the Montreal Protocol can be evaluated, provided that reliable data of stratospheric O₃ / temperatures and CRs are used.

Here, new quantitative analyses of polar stratospheric O₃ and cooling data in terms of the CRE mechanism are given with two improvements. First, atmospheric dynamics is known to cause large fluctuations in total O₃ in the polar hole from year to year.⁶⁶ To minimize this unpredictable short-term effect, a *three-point (year) adjacent averaging* is applied to observed data: $[O_3]_i = \{[O_3]_{i-1} + [O_3]_i + [O_3]_{i+1}\} / 3$. This minimal processing can effectively reduce the fluctuation level of measured data. Second, *statistical correlation* analyses between the CRE equation and observed data of total O₃ and stratospheric cooling over Antarctica are given here. Also note that the 2002 Antarctic stratospheric O₃ and temperature data, which showed large deviations and could generate artificial analysis results due to the unusual split of the polar vortex,⁶⁶ are excluded in the present analyses.

NASA's TOMS and OMI satellite datasets have so far provided the most widely used global and polar-area total O₃ data since 1979, while NOAA's ongoing surface-based observations have provided a measure of ozone-depleting chlorine and bromine containing gases in the lower atmosphere. Cosmic ray measurements at McMurdo (77.9° S, 166.6° E) are the only record providing continuous time-series CR data over Antarctica since 1960s. Here, the CR data at McMurdo and NOAA's EECI data measured in the lower atmosphere at Antarctica and mid-latitudes are plotted in Fig. 5A and B, respectively, which show that the tropospheric EECIs have declined since its peak observed around 1994. Indeed, the observed tropospheric EECI over Antarctica, normalized to the 1980 value, has declined by about 24% from the peak value. The NASA's October monthly mean total O₃ data calculated from 5° zonal-mean observed data with area weighted over the South Pole (60-90° S) and annual mean total O₃ in low- and mid-latitudes (65° S-65° N) in 1979-2010, as well as their 3-year average data, are shown in Fig. 5C and D, respectively. The observed data in Fig. 5C show that the Antarctic total O₃ decreased drastically from the end of the 1970s to 1995, following the significant rise of the halogen loading in the stratosphere. From 1995 to the present, total O₃ over Antarctica has exhibited pronounced 11-year cyclic oscillations. Total ozone at the mid-latitudes has shown a much smaller magnitude of *continuous* decrease and clear 11-year cyclic modulations since 1979 up to the present (Fig. 5D).

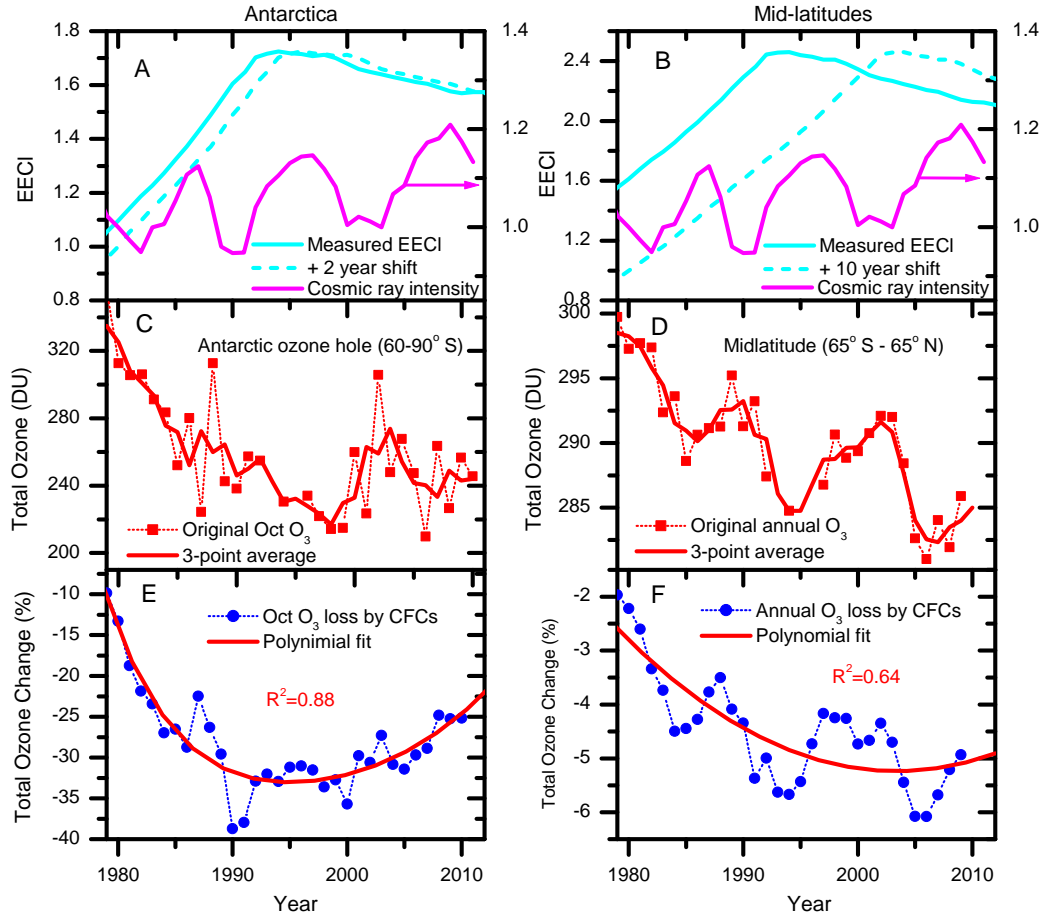


Figure 5. Observed and corrected time-series total ozone in Antarctica (60-90° S) and mid-latitudes (65° S-65° N) during 1979-2010. A and B: NOAA's equivalent effective chlorine (EECI) data measured in the troposphere (solid lines) and projected EECI in the stratosphere (dash lines) at Antarctica and mid-latitudes, as well as CR intensities I measured at McMurdo, Antarctica. Both stratospheric EECI and CR data are normalized to their values in 1980. C and D: October monthly mean total O_3 over Antarctica and annual mean total O_3 at mid-latitudes, obtained from NASA TOMS N7/M3/EP/OMI satellites; also shown are the 3-point adjacent averaged smoothing. E and F: 3-point mean total O_3 data are corrected by the CR-factor of $1/(I/I_{i-1})$; polynomial fits to the corrected data give coefficients of determination R^2 indicated and $P < 0.0001$ for $R^2 = 0$ (no trend). It is clearly discovered that after the CR effect is removed, the O_3 hole over Antarctica has recovered by 20~25%, while no clear recovery in O_3 depletion at mid-latitudes has been seen.

The observed Antarctic and non-polar O_3 data after correction by the CR-factor of $1/(I/I_{i-1})$ are shown in Fig. 5E and F, respectively, in which polynomial fits to the data give $R^2=0.88$ and 0.64 (coefficient of determination) with the probability $P < 0.0001$ for $R^2 = 0$ (no trend). Most strikingly, Fig. 5E shows that O_3 losses in the Antarctic hole have had a clear recovery since around 1995. Quantitatively, the October mean total O_3 loss over Antarctica has recovered by 20~25% from the peak loss at ~1995. Comparing the O_3 data in Fig. 5E with the EECI data in Fig. 5A, one can find that the corrected O_3 loss over Antarctica follows the NOAA measured EECI closely, with a short delay of only 1~2 years in the polar stratosphere. Indeed, the projected EECI with a 2-year delay has shown an approximately 23% decline from its peak at 1995-1996. This result indicates that CFCs are indeed one of the main causes of the Antarctic O_3 hole, which has shown a sensitive response to the decrease in the

tropospheric CFCs regulated by the Montreal Protocol. In contrast, Fig. 5F shows no sign in recovery for O₃ loss at the mid-latitudes. This means that a time delay of ≥ 10 years between the surface-measured and stratospheric EECl in the mid-latitudes is required, as shown in Fig. 5B. Thus, it is obvious that the stratospheric EECl decline and associated O₃ recovery in the mid-latitudes are significantly delayed, compared with those in the polar stratosphere.

In photochemical models, the 11-year cyclic variation of total O₃ in the tropics and midlatitudes was attributed to the pure solar cycle effect: maxima in UV solar irradiance cause maxima in photochemical O₃ production.⁶⁶ This explanation, however, ignores another prediction of the photochemical models: maxima in UV solar irradiance would lead to maxima in activation of halogens for O₃ destruction. It should be noted that in the past 3 solar cycles, UV solar irradiance varied at the Herzberg continuum (200–242 nm) by $\sim 3\%$ relevant to O₃ production, which is far less than $\sim 8\%$ at the Schumann–Runge bands (175–200 nm) and 18% at the Schumann–Runge continuum (130–175 nm) relevant to CFC photodissociation leading to O₃ destruction.⁸⁸ Furthermore, the photochemical models gave the maximum 11-year O₃ variation in the *upper* stratosphere at ~ 40 km, while the observed total O₃ cyclic variation originates mainly in the *lower* stratosphere at altitudes below 25 km for midlatitudes and the origin remains uncertain.⁶⁶ If the solar cycle effect is significant, a similar amplitude for total O₃ variations over the Northern and Southern Hemispheres (NH and SH) would be expected. However, when annual total O₃ in 0–65°S and 0–65°N bands obtained from the same NASA TOMS/OMI satellite datasets are plotted (not shown here), one can show that the total O₃ over the SH shows a much more pronounced 11-year variation than that over the NH. The latter actually shows a near flat in 1983–2004. This observation does not agree with the solar cycle effect, which cannot be the dominant origin. A more reasonable explanation seems that the cyclic total O₃ variation in the extra-polar region is due to the export of CRE-driven O₃ loss in the polar region; CRs have an 11-year cyclic variation by about 20% from solar minima to maxima (Fig. 5A). This effect exists in both hemispheres but is larger in the SH due to the larger and more regular O₃ depletion in the Antarctic vortex.⁶⁶ Note that no correction of total O₃ in the *polar region* by the UV solar irradiance has been proposed, as severe polar O₃ loss occurs mainly in the winter and early spring *lower* polar stratosphere at altitudes of 15–20 km and no solar effect is expected there.^{66,67} This is also evident by the fact that polar total O₃ observed in the *summer* Antarctic stratosphere showed no 11-year periodic variation, indicating no solar cycle effect on polar O₃ production.⁷ Finally, there is no significant trend in the *long-term* variation of solar irradiance since the 1970s,^{66,88} so no solar effect on the *long-term* trend of ozone in either polar or the extra-polar region is expected.

Moreover, the photodissociation mechanism proposed that CFCs would mainly decompose in the upper tropical stratosphere; air carrying the photoproducts (inorganic species) is then transported to the Antarctic stratosphere. Thus, a long delay (~ 6 years) from the troposphere peak was projected for the EECI to destroy O_3 in the Antarctic stratosphere.^{66,67} The situation for the mid-latitudes of both hemispheres is different from the Antarctica primarily because it was thought that air in the mid-latitude stratosphere would have a younger mean ‘stratospheric age’ (~ 3 years) compared to air above Antarctica. As a result, halocarbons in the mid-latitude stratosphere would need less time to become degraded by UV sunlight, and hence the EECI in the mid-latitude stratosphere was shifted by ~ 3 years only from the values measured at the troposphere.^{66,67} This understanding of halocarbons in the atmosphere is just opposite to the observed data shown in Fig 5. In contrast, the CRE mechanism gives that halocarbons are mainly *in-situ* destroyed in the *polar* stratosphere and therefore the EECI to destroy O_3 in the polar region should be more sensitive to the change of halocarbons in the troposphere. That is, a short delay (1–2 years) is expected between the polar stratospheric EECI change and the halocarbon change observed in the troposphere. Differently due to the low electron density in the mid-latitude stratosphere (see, Fig. 3A), the CRE-induced dissociation of halocarbons to destroy O_3 is a much slower process. In other words, halocarbons have a much longer residence time in the mid-latitude stratosphere than in the polar stratosphere. As a result, a much longer lag time from the tropospheric halocarbon change is expected for the EECI and resultant ozone recovery in the mid-latitude stratosphere. The observed data in Fig. 5 are therefore consistent with the CRE mechanism.

To establish the reliability of the above conclusions, statistical correlation analyses of the CRE mechanism and observed ozone data are shown in Fig. 6A-D, which plot the time-series October monthly mean and 3-month (October-December) mean total O_3 data observed by NASA satellites and fitted by Eq. 2 as well as total O_3 changes versus the product of $[C_i] \times I_i I_{i-1}$, respectively. First, as we expect, the 3-point adjacent averaging reduces the fluctuation level of total O_3 data significantly. Second, Figs. 6A and B show that Eq. 2 can well reproduce 11-year cyclic ozone losses in the Antarctic ozone hole. Third, Figs. 6C and D show that for the October and the 3-month average total O_3 data, statistical correlation coefficients -R of 0.86 and 0.92 are obtained for the linear fits to the observed data. All the statistical fits were made at a fixed 95% confidence. These results show an excellent linear correlation between total O_3 and the value of $[C_i] \times I_i I_{i-1}$ in the Antarctic O_3 hole and thus provide convincing evidence of the CRE mechanism (Eq. 2) and the reliability of the conclusions drawn from the observed ozone data corrected by $1/I_i I_{i-1}$ (Fig. 5).

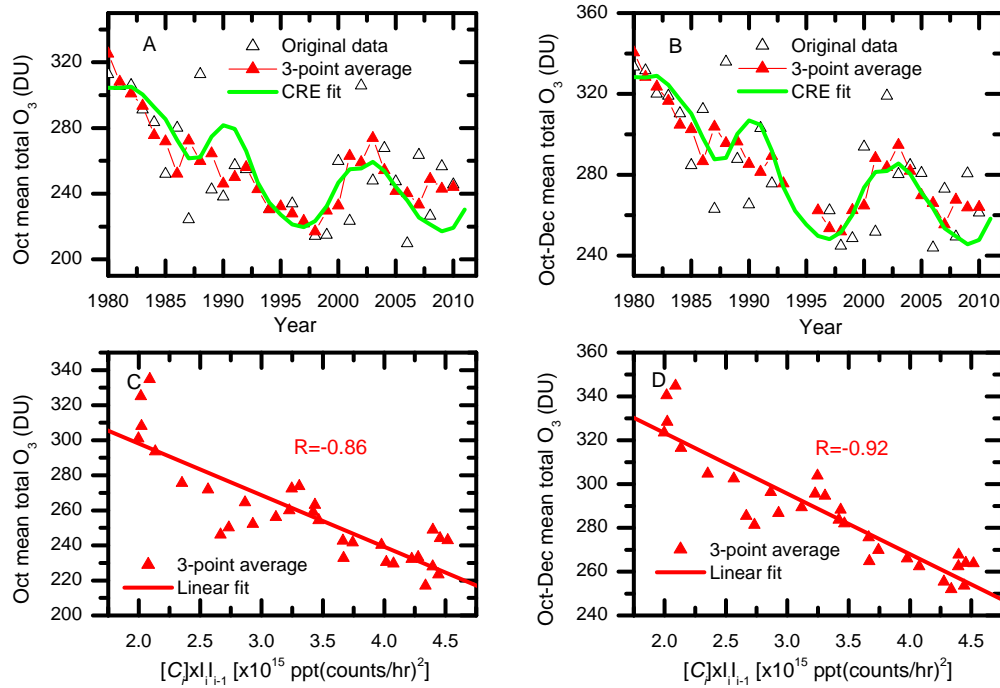


Figure 6. Statistical analyses of the CRE mechanism and the Antarctic (60-90° S) ozone hole during 1980-2010. A and B: Time series data of October mean and 3-month (October-December) mean total O₃ and their 3-point adjacent averaged data, as well as the best fits by the CRE equation (Eq. 2, text). C and D: 3-point average total O₃ data are plotted as a function of the product of $[C_i] \times I_i I_{i-1}$, the equivalent effective stratospheric chlorine $[C_i]$ and the CR intensities I_i and I_{i-1} in the current and preceding years; linear fits to the data give high linear correlation coefficients -R up to 0.92 and $P < 0.0001$ (for $R = 0$). Here, total O₃, EEC1 and CR data have the same sources as those in Figure 5.

As mentioned above, the temperature variation at the springtime lower polar stratosphere directly reflects real polar ozone loss. Thus, it is worthwhile to show the time-series variation of the lower polar stratospheric temperature. Here, both total ozone and temperatures in the lower stratosphere (100 hPa) at the BAS's Halley station (75°35' S, 26°36' W), Antarctica in the later springs (November, immediately after the O₃ hole peak in October) from 1979 to 2011 are shown in Fig. 7A. First, the observed data indeed visibly show that both total ozone and lower stratospheric temperature have *11-year cyclic variations*, which can be well fitted with Eq. 2 derived from the CRE mechanism. It is particularly interesting to note that the observed temperature data have a nearly perfect fit with Eq. 2. Second, Fig. 7B shows that the lower stratospheric temperature indeed has an excellent linear dependence on total ozone, in which a high correlation coefficient $R = 0.93$ is obtained. Third, the observed total O₃ and lower stratospheric temperature data after correction by the CR-factor of $1/I_i I_{i-1}$ are shown in Fig. 7C and E, in which polynomial fits to the data give $R^2 = 0.93$ (coefficient of determination) with the probability $P < 0.0001$ for $R^2 = 0$ (no trend). Consistent with the NASA satellite O₃ data for the Antarctica (60-90° S) in Figs. 5 and 6, both total O₃ and lower stratospheric temperature data at Halley again show a clear recovery since ~1995. Quantitatively, the pronounced recoveries of ~25% in total O₃ loss and of ~22% in stratospheric cooling have been clearly revealed.

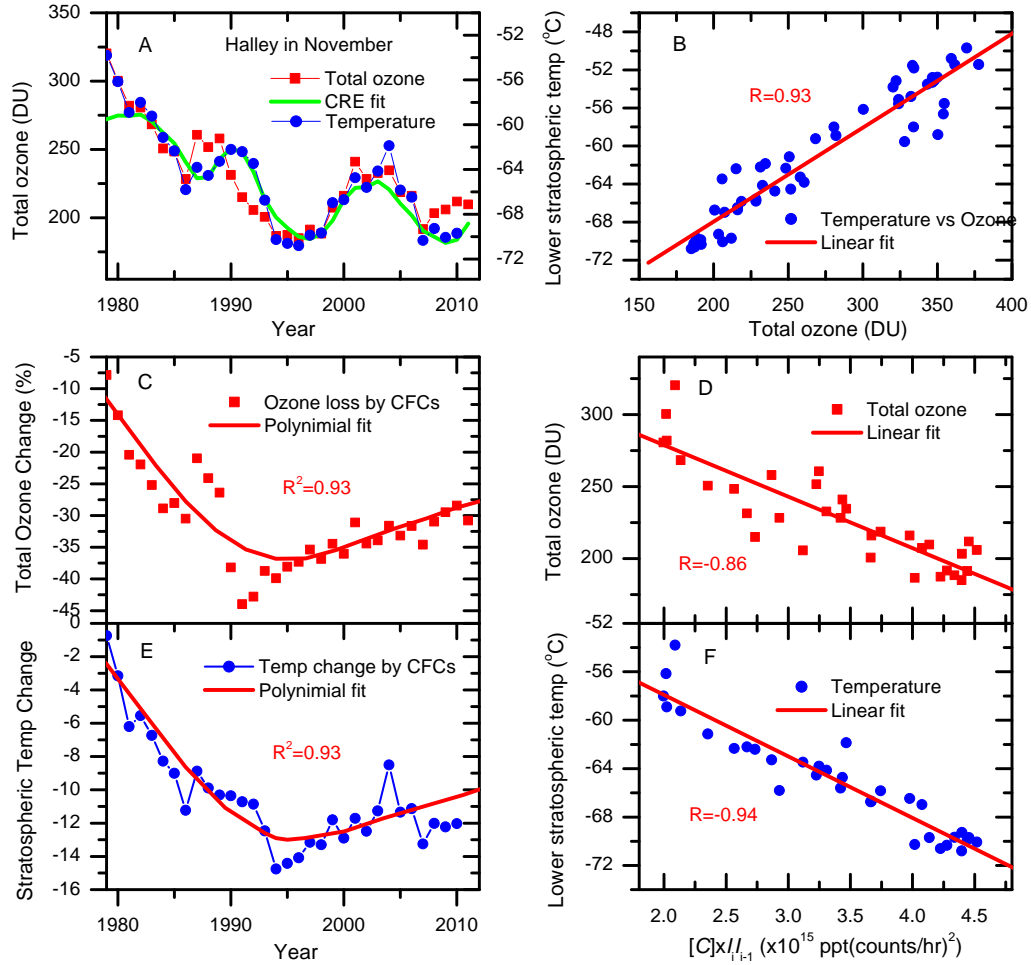


Figure 7. Observed and corrected time-series data and statistical analyses of total ozone and lower stratospheric temperature at Halley, Antarctica in November during 1979-2011. A: Observed time-series O_3 and temperatures (only a minimum 3-point smoothing was applied to the observed data), as well as the best fit by Eq. 2. B: Temperatures versus total O_3 ; a linear correlation coefficient R as high as 0.93 is observed. C and E: Observed O_3 and temperature data are corrected by the CR-factor of $1/(I_{i-1})$; polynomial fits to the correct data are also shown. It is clearly revealed that O_3 loss at Halley has recovered by about 25%. D and F: O_3 and temperature data are plotted as a function of the product of $[C_i] \times I_{i-1}$, respectively; linear fits to the data are also shown. High linear correlation coefficients ($-R$) up to 0.94 are obtained.

Fourth, statistical correlation analyses of total ozone and lower polar stratospheric temperature at Halley in terms of the CRE equation are shown in Figs. 7D and F, respectively. Again, excellent linear correlations of total O_3 and stratospheric temperature with $[C_i] \times I_{i-1}$ variations are observed, and *high linear correlation coefficients* $-R$ up to 0.94 and $P(\text{for } R=0) < 0.0001$ are obtained. Similar to those shown in Figs. 6A-D, these results in Figs. 7A-F confirm that the CRE mechanism can excellently reproduce not only total O_3 but also O_3 -loss-induced stratospheric cooling data in the Antarctic hole. The observed pronounced 11-year cyclic variations in total O_3 and lower stratospheric temperature are obviously due to the effect of CRs. These results lead to an important conclusion that both polar O_3 loss and lower stratospheric temperature over the past decades are well described by Eq. 2 with the equivalent effective stratospheric chlorine $[C]$ and the CR intensity I as the only two variables. *In particular, the strikingly high linear correlation coefficient of 0.94 indicates that the long-term*

temperature variation in the lower polar stratosphere is nearly completely controlled by Eq. 2. This is in striking contrast to the prediction of previous climate models that the magnitude of stratospheric cooling due to the CO₂ increase would be as large as that induced by O₃ loss.⁷⁹ As a matter of fact, the results in Figs. 5-7 show no effect of non-halogen GH gases (CO₂, CH₄, N₂O, etc) on the stratospheric climate of Antarctica over the past four decades.

In a short summary, the excellent statistical correlations of total O₃ and polar stratospheric cooling with $[C_i] \times I_{i-1}$ in the Antarctic O₃ hole shown in Figs. 5-7 have given high confidence in applying Eq. 2 to unravel the direct effect of human-made CFCs on O₃ loss. After the removal of the effect of CRs by correcting the observed data with the CR-factor of $1/(I_{i-1})$, both O₃ loss and stratospheric cooling in the polar O₃ hole have shown a clear recovering trend since around 1995, closely following the decrease of CFCs with the peak measured in the troposphere that occurred in 1993-1994. *A pronounced recovery by 20~25% of the O₃ hole is now clearly revealed.* This result shows the success and importance of the Montreal Protocol inhibiting the use of CFCs on a global scale.

VI. Future Trends of the Ozone Hole

The high correlation coefficients obtained in Figs. 6 and 7 has indicated the validity of Eq. 2. This gives confidence in applying Eq. 2 to predict the future recovery of the ozone hole with the projected variations of human-made EECl and natural CRs. The Montreal Protocol has been effective in regulating ozone-depleting halogen-containing molecules, so that the EECl in the polar stratosphere is expected to continue the decreasing trend that has been observed in the past decade.⁶⁷ The CR-intensity variation with an average periodicity of 11 years and its modulation of ~10% are well known, which can generally be expressed as⁷

$$I_i = I_{i0} \left\{ 1 + 10\% \sin \left[\frac{2\pi}{11} (i - i_0) \right] \right\}, \quad (4)$$

where I_{i0} is the median CR intensity in an 11-year cycle. Note that I_{i0} at Antarctica in the past three solar (CR) cycles has an increasing rate of ~2% per 11-year cycle. The best fit to all the observed CR data at the Antarctica (McMurdo) from 1960s-2009 yielded $I_{i0} = 8800[1 + 2\%(i - 1979)/11]$ (10^2 count/hr).⁷ However, there is some uncertainty for the future change of solar activity, which regulates the future change of CRs in the coming decades. Here, we discuss three possible scenarios: A, the mean CR intensity (I_{i0}) in the solar cycles in the 21th century would keep the same rising rate as that in the past three solar cycles; B, I_{i0} would keep nearly a constant value identical to that observed for the

last 11-year cycle (2000-2011); and C, I_{i0} would have a decreasing trend returning to the value in 1970. The future CR intensities calculated by Eq. 4 with these scenarios of I_{i0} are shown in Fig. 8A. With these projections and the projected EECI data obtained with a lag time of only 2 years from the tropospheric EECI data, the calculated October and October-December total O_3 over Antarctica for 1980-2080 by Eq. 2 are shown in Figs. 8B and C. The Antarctic O_3 hole is predicted to recover to the 1980 level around 2058(± 5), depending on the variations of not only the halogen loading but also CRs in the stratosphere. This recovery is faster by about 30~40 years than that given by photochemical model calculations,⁶⁷ which predicted a recovery to the pre-1980 value by the end of this century.

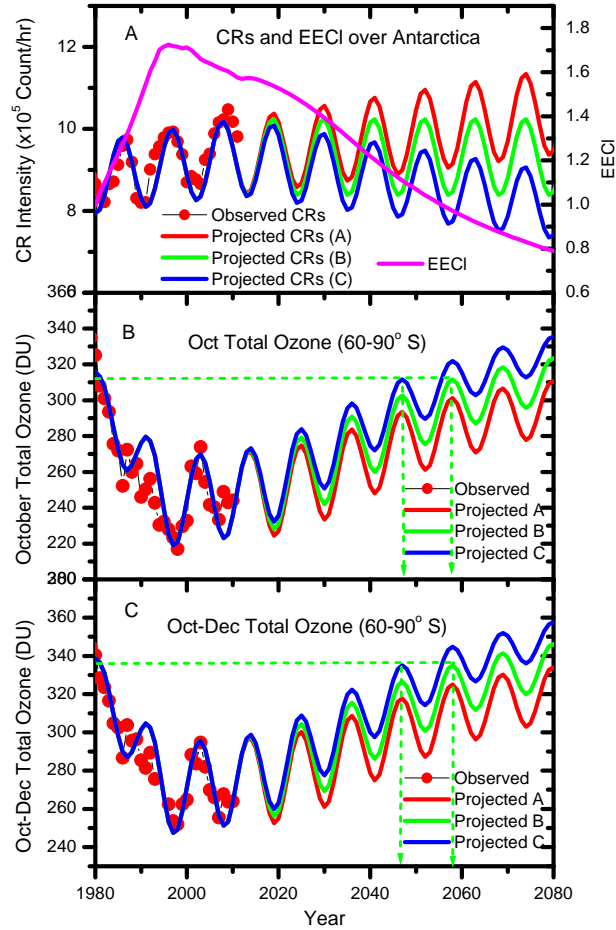


Figure 8. Future trend of the Antarctic ozone hole. A: Observed and projected future changes of cosmic ray (CR) intensity and the equivalent effective chlorine (EECI) in the stratosphere of Antarctica, where projected EECI data were obtained with an assumed lag time of 2 years from the measured tropospheric EECI data over Antarctica, observed CR data up to 2011 were obtained from the measurements at McMurdo and the future CR data were projected by Eq. 4 with the three possible scenarios of I_{i0} given in the text. B and C: Calculated October monthly mean and 3-month (October-December) mean total O_3 over Antarctica with latitudes (60-90° S) by Eq. 2 with the observed and projected EECI and CR data shown in A; the observed total O_3 data (solid circles in red) from 1979 to 2010 are the same as those in Figure 6. The projected time range for recovery of the Antarctic O_3 hole to the 1980 level is also indicated (arrows).

VII. Natural Effects on Global Surface Temperature

There has been intense debate on the natural effect on Earth climate over the past 3~4 solar cycles. The controversies arise partially from the fact that direct total solar irradiance (TSI) measurements have only been available during the last three cycles and are based on a composite of many different observing satellites. As reviewed recently by Fröhlich,⁸⁹ there are some differences in constructed TSI composites in not only absolute TSI values but also time-series trends of TSI. Two representative TSI composites are the PMOD composite⁵⁶ and the ACRIM composite⁵². Both are discussed in detail in their corresponding team websites. The ACRIM composite used the data as published, whereas the PMOD composite introduced corrections of effects not considered in the original data analysis. The ACRIM composite TSI time series showed an upward trend of 0.04-0.05% per decade between consecutive solar activity minima and was proposed to account for the global temperature rise in recent decades.⁵² In contrast, the PMOD TSI composite showed a downward trend of TSI at solar maxima and indicated that the measured TSI variations since 1978 are too small to have contributed appreciably to accelerated global warming over 1970-2000.⁵⁶ Other studies^{54,55,57} have shown that the solar activity cannot have had a significant influence on global climate since ~1970, irrespective of the specific process dominant in determining Sun-climate interactions: TSI changes or solar UV changes or cloud coverage changes by CR flux variations. Lockwood and Fröhlich⁵⁷ have even concluded that all the trends in the Sun for either a direct TSI effect on climate or an indirect effect via CR-regulated cloud coverage or for a combination of the two have been in the opposite direction to that required to explain the observed rise in global temperature in the late 20th century.

Here, observed global surface temperatures and observed and constructed TSI composites since 1850 are shown in Fig. 9. In fact, one can see that overall the difference in the long-term TSI variations of the PMOD and ACRIM composites is not significant as far as the mean TSI trend is concerned, though the TSI minima are slightly different between the two composites. In the past 3 solar cycles, the mean TSI variation has been insignificant, compared with the significant rising trend in 1900-1950 and the decreasing trend in 1950-1965. If the correlation of TSI and global surface temperature after 1970 remains the same as that prior to 1970, global temperature change due to the variation of the mean TSI since 1970 is negligibly small. Thus, it seems reasonable to make a rough conclusion that the mean TSI variation in either of the PMOD and ACRIM composites could not explain the significant global temperature rise from 1970 to 2002.

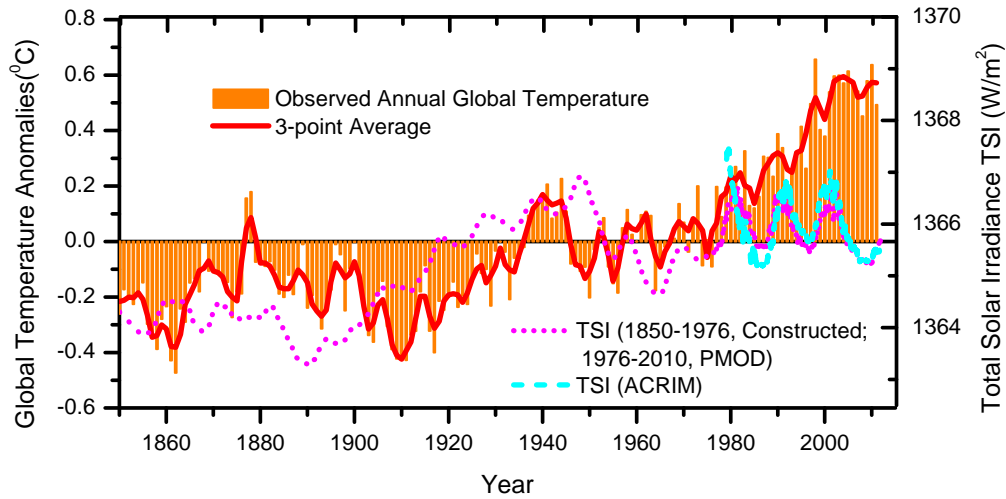


Figure 9. Possible natural effects on global surface temperature. Time-series annual global (combined land and sea) surface temperature anomalies in 1850-2011 were from the UK Met Office; the red curve is a 3-point average of observed data. Time series total solar irradiance (TSI) constructed based on models and proxies prior to 1976 (ref. 50) and on direct measurements after 1976 (PMOD TSI; ACRIM TSI), where their absolute values are shifted to equal in the 1970s. The right y-axis scale range for TSI data is adjusted to show their similarity to global surface temperatures prior to 1970.^{50,54}

To reach a more robust conclusion on the potential Sun's influence on climate since 1970, a more delicate analysis of indices of solar activity is required. Fortunately, observational records of the sunspot number (SSN) began about 300 years ago, and there has been little disagreement about the observed data of SSN. Approximately every 11 years, a maximum of solar activity is reached, with a large number of sunspots present on the solar surface. Solar cycle activity maxima are separated by minima during which only a few or no sunspots are present on the solar surface. As an indicator of solar activity, the number of sunspots is expected to have a consistent behaviour with TSI. Moreover, the cosmic-ray intensity modulated by the strength of the Sun's open magnetic field is another indicator of solar activity and has been well recorded by independent detection stations in many parts of the world since the 1950s; the data are available from the Network of Cosmic Ray Stations. Thus, with combined measured data of TSI, SSN and the CR intensity from multiple sources, it is possible to obtain a reliable evaluation of the solar effect on the Earth's climate since 1970. Here, for comparison the PMOD and ACRIM TSI composites are again plotted in Fig. 10A, while the recorded time-series data of the SSN since 1900 are plotted in Fig. 10B. Fig. 10C shows the CR intensities since the 1950s from measurements *at ten stations* (McMurdo, Moscow, Apatity, Inuvik, Oulu, Kiel, Cape, Thule, Climax and Newark) at various altitudes (0-3 km) and latitudes from the polar regions to mid-latitudes. It can clearly be seen from Fig. 10B that the mean SSN had a rising trend in the first half of the 20th century and a declining trend after that, particularly in the past 3 solar cycles. The variation of the CR intensity should be anti-correlated with that of the solar activity: the solar activity minimum (maximum)

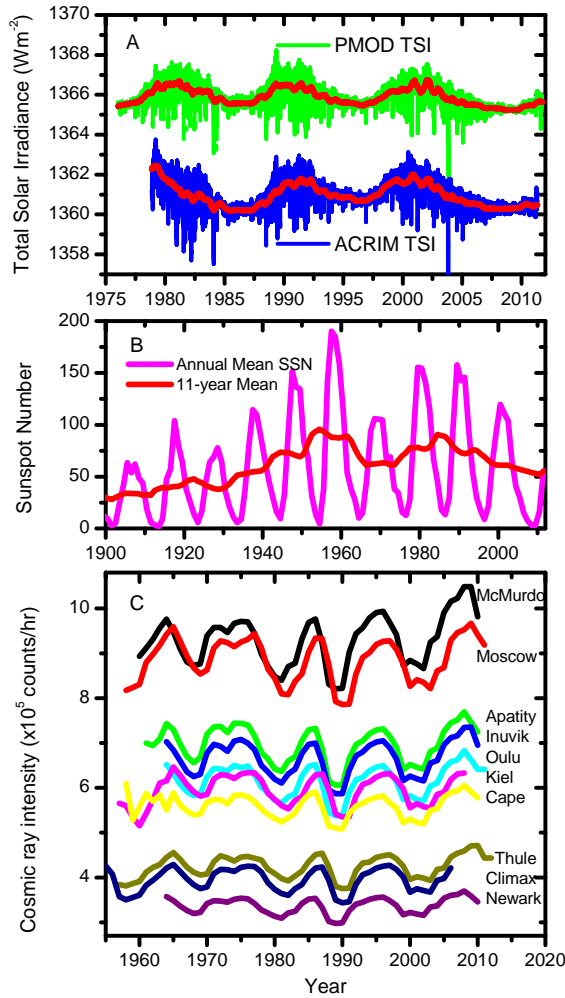


Figure 10. Time series variations of the indicators of solar activity. A: PMOD and ACRIM TSI composites constructed from measurements since 1976/1978. B: Annual mean sunspot number (SSN) and 11-year average sunspot number (SSN) from 1900 to 2011. C: Annual Mean cosmic ray intensity data measured at ten neutron detector stations (McMurdo, Moscow, Apatity, Inuvik, Oulu, Kiel, Cape, Thule, Climax and Newark) from the 1950s to 2011.

corresponds to the CR maximum (minimum). As shown in Fig. 10C, indeed, the observed CR data from multiple stations show that the *overall mean CR intensity has had an increasing trend during the period of 1970 up to the present*. Clearly, the observed CR maximum at 1997 is slightly larger than that in 1986. This is opposite to the expectation from the ACRIM TSI composite⁵² showing that the TSI minimum at 1997 is larger than that at 1986, while consistent with the PMOD TSI composite^{56,89}. Overall, the combined time series data of TSI, SSN and CR intensity in Fig. 10 have unambiguously shown that the natural influence on climate is indeed in the opposite direction to that required to explain the observed rise in global temperature in the decades of 1970-2002. That is, the natural effect is negligible and the human effect must be dominant. This conclusion, which is consistent with recent studies,⁵⁴⁻⁵⁷ is now clearly established by the substantial observed data shown in Fig. 10.

VIII. Global Surface Temperature vs CO₂ or CFCs

It was recently shown that global surface temperature remained nearly constant from 1850 to ~1930, while the recorded CO₂ level had been rising since 1850.³⁵ When global temperature was plotted versus CO₂ concentration, it gave a nearly zero correlation coefficient $R (=0.02)$, that is, the global temperature was independent of the rising CO₂ level (285 to 307 ppm) over this 80 year period.³⁵ Here, Figs. 11A-F show observed data of CO₂, halocarbons and global surface temperature in the periods prior to and after 1970, corresponding to the atmospheres without and with appreciable anthropogenic CFCs. Time-series data of atmospheric CO₂ concentration and global surface temperature from 1850 to 1970 are plotted in Fig. 11A. During this period of 120 years, global temperature versus CO₂ concentration is plotted in Fig. 11B. Indeed, it is clearly seen that the observed global temperatures were almost independent of the CO₂ concentration rise (285-326 ppm). There was a significant temperature jump in the short period of 1930-1940, but this can be explained well by the significant rise in solar activity,^{50,54} as shown in Fig. 9. Time-series data of atmospheric CO₂ concentration, the total concentration of major atmospheric halocarbons (CFCs, CCl₄ and HCFCs) and global surface temperature over the four decades from 1970 to 2011 are plotted in Figs. 11C and E. In Fig. 11C, it is particularly interesting to show that both the CO₂ concentrations and the total halocarbon concentrations had a nearly identical growth shape during the three decades from 1970 to ~2000, while they have been drastically different since the beginning of this century. Namely, the CO₂ has kept the identical rising rate, whereas the total halocarbon concentration has had a turnover since ~2002. Correspondingly, it is clearly shown in Fig. 11E that global surface temperature had a linear rise from 1975 to ~2002 and has had a slowly declining trend since 2002. The 3-point smoothed temperature data in Fig. 11E also exhibits visible, 11-year cyclic small modulations, which can be attributed to the solar effect or stratospheric cooling arising from ozone loss caused by CFCs and CRs or the combination of the two effects.

Most interesting are the results shown in Figs. 11D and F plotting global temperature as a function of CO₂ concentration and total concentration of halocarbons, respectively. In Fig. 11F (and Fig. 11C), a 9-year delay in halocarbon concentrations in the stratosphere from surface-based measurements must be applied, otherwise, global surface temperature would show a sharp rise with high total halocarbon concentrations above 1100 ppt (1.1 ppb).^{7,35} This delay of 9 years on the average in *global* stratospheric halocarbons was not explained previously. It has now been justified by the observation shown in Fig. 5 that the stratospheric EECI delays in the polar region (60°-90° S) and in the non-polar latitudes (65° S-65° N) are 1~2 and ≥10 years from surface-measured EECIs, respectively. Strikingly,

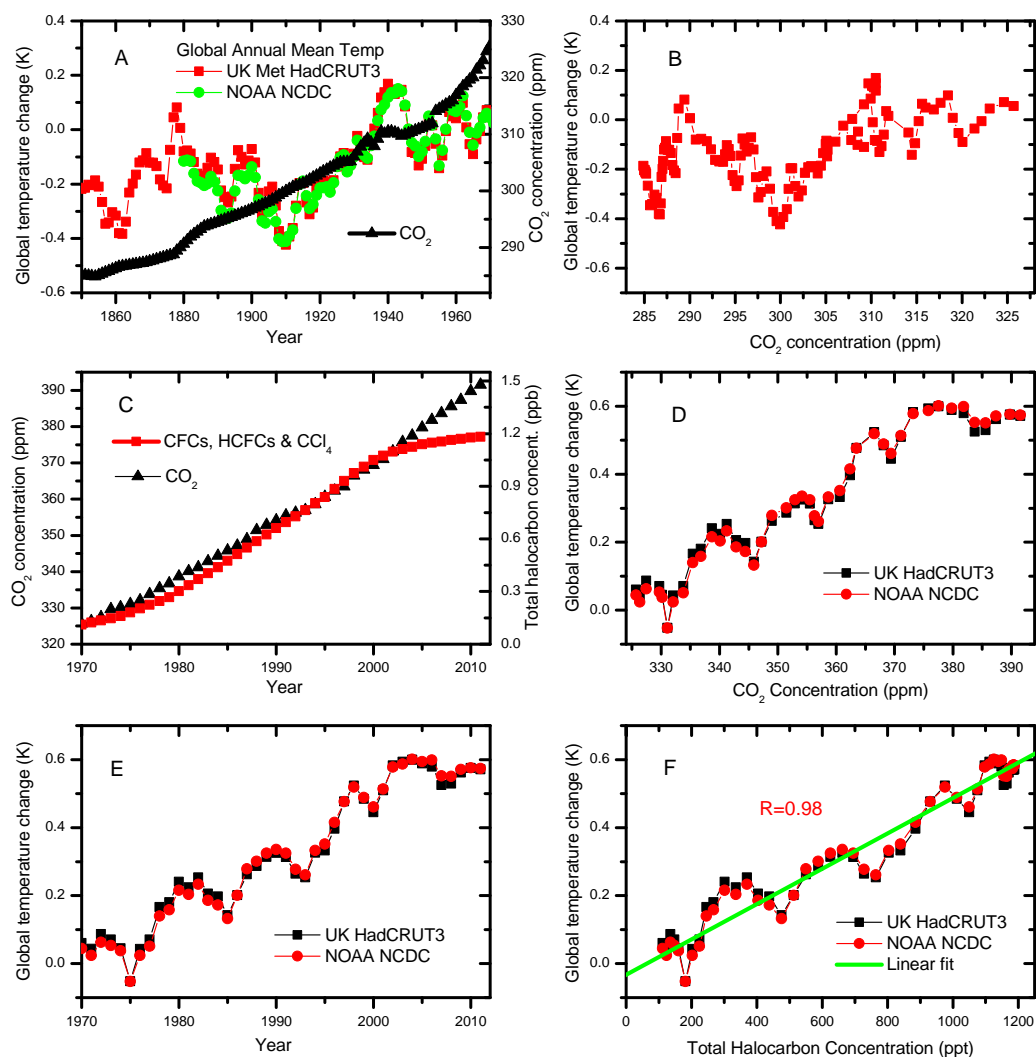


Figure 11. Global surface temperature, CO₂ and halocarbons from 1850 to 2011. A and B for 1850-1970: Time-series atmospheric CO₂ concentrations and global surface temperatures (A); global surface temperature versus atmospheric CO₂ concentration (B). C-F for 1970-2011: Time-series atmospheric CO₂ concentrations and total concentrations of atmospheric halocarbons (CFCs, HCFCs and CCl₄) (C); Time-series global temperatures (E); Global temperature versus CO₂ concentration (D); Global temperature versus total concentration of atmospheric halocarbons (F). A linear fit in F gives a nearly unit correlation coefficient $R=0.98$ with $P<0.0001$ for ($R=0$). CO₂ data from 1850 to 1958 were from the Law Dome ice core analysis and data after 1958 were from direct atmospheric measurements at Mauna Loa Observatory. For halocarbon concentrations in the stratosphere, a 9-year delay from surface-based measurements was applied (see the text). Annual global surface temperatures (combined land and ocean (sea) surface temperature anomalies) were from both the UK Met Office and the US NOAA; only a minimum 3-point smoothing was applied to observed temperature data. The UK HadCRUT3 data are shifted by 0.145 °C to overlap with the NOAA data.

Fig. 11F shows that global surface temperature has had a nearly perfect linear dependence on the total amount of atmospheric halocarbons from the 1970 to the present. Statistically, the linear fits to the UK Met Office data and NOAA data give statistical linear correlation coefficients R as high as 0.97 and 0.98 (close to unit) and $P<0.0001$ for $R=0$, respectively. In contrast, Fig. 11D shows that global temperature appeared to have a linear increase at the CO₂ concentrations of 326-373 ppm (1970-2002), but it started to decrease with rising CO₂ levels of 373-392 ppm (2002-2011).

The above observed data strongly indicate that global temperature is highly sensitive to the variation of atmospheric halocarbons rather than increasing CO₂ and other non-halogen GH gases. For a GH gas, the calculation of the radiative force change ΔF with changing concentration can be simplified into an algebraic formulation that is specific to the gas. In IPCC climate models,^{66,67,83,84} a *linear* dependence of the ΔF with concentration has been used for halocarbons with low concentrations (e.g., a CFC in ≤ 1 ppb), whereas a *logarithmic* relationship has been assumed for CO₂ with high concentrations (>100 ppm) so that increased concentrations have a progressively smaller warming effect. Namely, the simplified first-order expression for the radiative force ΔF of CO₂ is:

$$\Delta F = 5.35 \times \ln(C/C_0) \quad (5)$$

in Wm^{-2} , where C is the CO₂ concentration in parts per million (ppm) by volume and C_0 is the reference concentration. With the CO₂ concentration rising from 285 ppm in 1850 (pre-industry era) to ~ 390 ppm by 2010, Eq. 5 gives the radiative forcing of $\sim 1.7 \text{ W/m}^2$ for CO₂ alone.⁶⁷ Eq. 5 would also give rise to an identical $\Delta F \approx 0.72 \text{ W.m}^{-2}$ for the CO₂ concentration rises of 285 to 326 ppm in 1850-1970 and 326 to 373 ppm in 1970-2002. This result indeed contradicts the observed temperature variations of $\sim 0.2^\circ\text{C}$ during 1850-1970 and of $\sim 0.6^\circ\text{C}$ during 1970-2002, not to mention the observed *negative* correlation with CO₂ at higher concentrations (≥ 373 ppm) since 2002. In contrast, the observed global temperature has exhibited a nearly perfect linear positive correlation ($R \approx 1.0$) with the total concentration of halocarbons since their considerable emission into the atmosphere in the 1970s. All these data strongly indicate that the GH effect of increasing non-halogen gases has been saturated and that halocarbons (mainly CFCs) have played the dominant role in global climate change since 1970.

IX. Refined re-evaluation of the Greenhouse Effect of Halocarbons

The change in equilibrium surface temperature (ΔT_s) arising from the radiative forcing ΔF of the surface-atmosphere system due solely to a GH gas increase can be calculated by:

$$\Delta T_s = \alpha \beta \Delta F, \quad (6)$$

where α is the *climate sensitivity factor* in $\text{K}/(\text{W/m}^2)$ defined as $\alpha = dT/dF$ and β is the *climate feedback amplification factor*. As global surface temperature rises, tropospheric water vapor increases and this represents a key positive feedback of climate change. It has been estimated that water vapor feedback

acting alone approximately doubles the warming from what it would be for fixed water vapour (i.e., $\beta \approx 2$).⁸⁴ Moreover, water vapour feedback may also amplify other feedbacks such as cloud feedback and ice albedo feedback in models. The latter is unclear, and there exists a large uncertainty in climate sensitivity factor α .^{83,84} Given no saturation in the GH effect of CO₂, the use of Eq. 5 with the current large atmospheric CO₂ concentration (~392 ppm) would give a very large radiative force (~1.7 W/m²).⁶⁷ Consequently, observed temperature changes forced climate models to use a very low climate sensitivity [$\alpha\beta \leq 0.5$ K/(W/m²)]. Unfortunately, this has inevitably led to the general conclusion that halocarbons are important, but by no means dominant for surface temperature changes.^{66,67,79,82-84}

For a GH gas at low concentrations (≤ 1 ppb) such as CFCs and HCFCs, ΔF has a simple linear dependence: $\Delta F = \chi C$, where C is the concentration of the GH gas and χ in Wm⁻² ppb⁻¹ is the radiative efficiency that refers to the radiation change at the tropopause caused by a given change in C .^{66,67,83,84} In fact, this linear dependence has now been well confirmed by the present observation of a nearly perfect linear dependence of global temperature on halocarbon concentration from 1970-2011, as shown in Fig. 11F. The χ values for halocarbons were calculated using radiative transfer models of the atmosphere and available in the WMO Report.⁶⁶ These values can be used to calculate the change ΔF as a function of changing GH concentration.

In view of the saturation in GH effect of non-halogen gases, simple model calculations of the global surface temperature change ΔT_s due solely to the GH effect of halocarbons have been made recently.³⁵ Here, a modification is made to include the 11-year cyclic small temperature modulations due to the solar/CR effect or the ozone loss effect caused by co-effects of CFCs and CRs or the combination of the two effects. In view of the observations presented in Section VII and previous studies⁵⁴⁻⁵⁷, showing that the solar effect plays only a very minor part in global surface temperature variations since 1950, a small modulation of 0.05 °C with an 11-year periodicity is simply assumed. This 11-year cyclic temperature variation is superposed onto the global temperature change induced by the greenhouse effect of halocarbons:

$$\Delta T_s = \Delta T_s(\text{Halocarbons}) + 0.05 \cos[2\pi(i-1992)/11]. \quad (7)$$

The resultant calculated global temperatures from 1950 to 2011 are shown in Fig. 12, together with the observed global surface temperatures since 1950. It can be clearly seen that the calculated results by Eq. 7 can reproduce well the observed temperature data in 1950-2011. Here, the distinction from previous climate model calculations^{79-84,66,67} is that the present calculations are based on the observed

saturation in the GH effect of non-halogen gases (CO_2 , CH_4 and N_2O) and consider the GH effect of halocarbons only. The results in Fig. 12 demonstrate that halocarbons (mainly CFCs) alone could indeed result in the observed global surface temperature rise of about 0.6°C in 1950-2002.

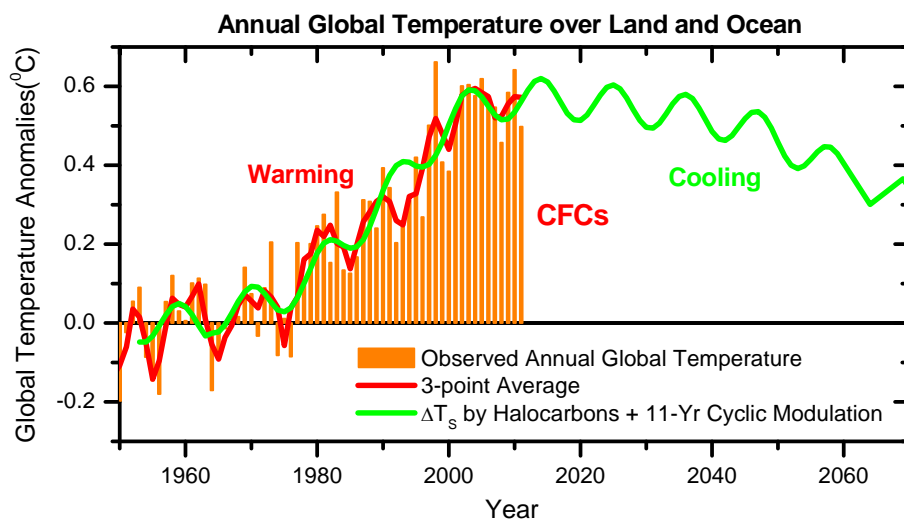


Figure 12. Natural and human effects on global surface temperature. Observed global surface temperatures were from the UK Met Office's combined land-surface air temperature and sea-surface temperature anomalies; the red curve is 3-point average of observed data. The equilibrium surface temperature changes (ΔT_s) (curve in green) were calculated by Eq. 7, including the contributions from the pure greenhouse effect of halocarbons (CFCs, HCFCs and CCl_4) obtained with a climate sensitivity factor $\alpha=0.9 \text{ K W}^{-1}\text{m}^2$ and a feedback amplification factor $\beta=2$ [ref. 35] and from an 11-year cyclic small modulation ($\pm 0.05^\circ\text{C}$) due to the solar activity (CR) related effect (see text).

X. Future Global Temperature Change

The above Sections have strongly indicated that CFCs are the major culprit for global climate change since 1950. Thus, the future climate change will be mainly governed by the variation of halogenated molecules in the atmosphere. With the projected concentrations of major halocarbons including CFCs, HCFCs and CCl_4 in the future,^{66,67} global surface temperatures due to halocarbons plus small 11-year cyclic modulations (within 0.05°C) in 2012-2070 have also been calculated and shown in Fig. 12. As revealed by the observed O_3 data shown in Fig. 5, the decline in the total halogen burden in global stratosphere, especially in the low and middle latitudes, is much slower than that in the polar stratosphere and is significantly delayed by about one decade from that measured in the troposphere. As a result, the recovery in global surface temperature will be much slower than that in the Antarctic O_3 hole. The global temperature is expected to return to its mean value in 1950-1970 by the end of 21st century. Certainly, the future global temperature change might be affected by the variation of solar activity. However, there is currently no sign that the solar effect would significantly affect the Earth climate in the coming decades.⁹⁰ Thus, there is good reason to expect that global surface temperature is reversing slowly with decreasing concentrations of CFCs in the atmosphere. It should

also be noted that similar to the temperature trend in the past decade, the Earth in the coming decade will still be in the hottest climate over the past 150 years. However, a long-term trend of global temperature recovery (cooling) is expected for the coming five to seven decades, as shown in Fig. 12.

XI. Future Global Sea Level Change

It is well known that the change in stratospheric ozone radiatively affects surface temperature.^{66,67} As shown in the Earth blackbody radiation intensity spectrum (Fig. 4), O₃ is an effective greenhouse gas due to its strong absorption at 9.6 μm . Currently, global stratospheric total O₃ in low- and mid-latitudes (65° S-65° N) has been depleted by about 6% (Fig. 5D). On the global scale, the negative radiative forcing of climate due to stratospheric O₃ depletion is only $-0.05 \pm 0.1 \text{ W/m}^2$, much smaller than the positive radiative forcing due to atmospheric CFCs and HCFCs causing the depletion.⁶⁷ However, severe ozone loss in the polar hole has largely affected many aspects of the surface climate over Antarctica, even Southern hemisphere mid- and high-latitudes. These include: the southward shift of the Southern hemisphere tropospheric jet, surface winds warming over the Antarctic Peninsula and cooling over the high plateau as well as observed increases in sea-ice area averaged around Antarctica over the past decades.⁶⁷ The present observation of a faster recovery in the Antarctic ozone hole than global surface temperature, corresponding to the observation that the decline of the total halogen burden in the polar stratosphere is much faster than that in global stratosphere, means that in spite of the expected decrease in future global temperatures, the averaged melting of sea ice around the polar region will *increase* in coming decades. This will lead to an interesting phenomenon that the global sea level will continue to rise while the global surface temperature slowly decreases in the coming one to two decades. This trend is expected to keep until the effect of the global temperature recovery dominates over the effect of the ozone hole recovery on the sea ice area. After that, both global surface temperature and sea level are expected to drop concurrently.

XII. Concluding Remarks

Numerous observations have robustly shown that both the natural effect (CRs) and the human effect (CFCs) contribute to the depletion in the O₃ layer. According to the CRE mechanism that has been strongly supported by many data from both laboratory and field measurements, ozone loss in the polar O₃ hole can be quantitatively expressed as: $-\Delta[\text{O}_3]_i = k[C_i]I_iI_{i-1}$, with the equivalent effective chlorine level $[C]$ in the polar stratosphere and the CR intensity I as variables. In this study, comprehensive time-series data sets of halocarbons, CRs, total ozone and O₃-loss-induced stratospheric cooling have

given excellent quantitative and statistical analysis results consistent with the CRE mechanism. After the removal of the CR effect, a pronounced recovery by 20~25% of the Antarctic O₃ hole since ~1995 is discovered, while no sign in recovery of O₃ loss in mid-latitudes has been observed. The polar O₃ hole has shown a sensitive response to the decline in total halogen burden in the low troposphere since 1994 due to the regulation by the Montreal Protocol. The CRE mechanism has well reproduced 11-year cyclic variations of the Antarctic O₃ hole and the associated stratospheric cooling and can significantly improve our predictive capabilities for future polar ozone loss.

Furthermore, the substantial combined data of total solar irradiance, the sunspot number and cosmic rays from multiple measurements have unambiguously demonstrated that the natural factor plays only a very minor effect on Earth's climate since 1970. Instead, the recent global warming observed in the late 20th century was mainly due to the greenhouse effect of human-made halocarbons (mainly CFCs). The re-evaluation has shown that halocarbons (mainly CFCs) alone accounted for the global temperature rise of about 0.6 °C in 1970-2002. Owing to the effectiveness of the Montreal Protocol, the globally mean halocarbon level in the stratosphere has entered a very slow decreasing trend since 2002. Correspondingly, a very slow declining trend in the global surface temperature has been observed. It is expected that the success of the Montreal Protocol will lead to a long-term slow return of the global surface temperature to its value in 1950-1970 for coming 50-70 years.

In conclusion, the observed data have shown that CFCs are the major culprit not only for O₃ depletion via conspiring with cosmic rays but also for global warming by ~0.6 °C during 1970~2002. The successful execution of the Montreal Protocol has shown its fast effectiveness in controlling the O₃ hole in the polar region and a slow cooling down of the global surface temperature. The O₃ loss in the polar region is estimated to recover to its 1980 value by 2058, faster than recently expected from photochemical model simulations,^{66,67} while the return (lowering) of global surface temperature will be much slower due to the slow decline of the stratospheric halocarbons in low and mid latitudes. This leads to an interesting prediction that global sea level will continue to rise in coming 1~2 decades until the global temperature recovery dominates over the O₃ hole recovery. After that, both global surface temperature and sea level will drop concurrently. It should also be noted that although the mean global surface temperature in the next decade will keep nearly the same value as in the past decade, i.e., “the hottest decade”, a slow cooling trend has begun (as shown in Fig. 12).

This study also shows that revealing the fundamental mechanisms underlying the ozone hole and global climate change requires correct understandings of the basic physics of cosmic ray radiation and the Earth blackbody radiation as well as their interactions with human-made molecules. When these

understandings are presented with observations objectively, reaching consensus on these scientific issues of global concern are feasible. Finally, this study points out that humans are mainly responsible for the ozone hole and global climate change, but international efforts such as the Montreal Protocol and the Kyoto Protocol must be placed on firmer scientific grounds. This information may be of importance to the research community, the general public and the policy makers.

Acknowledgements. The author is greatly indebted to the following Science Teams for making the data used in this study available: NASA TOMS and OMI Teams (especially Drs. P. K. Bhartia, R. McPeters, A. Krueger, J. Herman), NASA UARS's CLAES Team (especially Drs. A. E. Roche and J. B. Kumer), the British Antarctic Survey's Ozone Team (Dr. J. D. Shanklin), the University of Oxford's MIPAS team (Dr. Anu Dudhia), the Bartol Research Institute's Neutron Monitor Team (Dr. John W. Bieber) and the Network of Cosmic Ray Stations, the UK Met Office Hadley Centre, the US NOAA National Climatic Data Center (NCDC) and Global Monitoring Division, the US DOE Oak Ridge National Laboratory (ORNL)'s Carbon Dioxide Information Analysis Center (CDIAC), the Royal Observatory of Belgium's Solar Influences Data Analysis Center (SIDC), the Swiss PMOD / WRC team (Dr. Claus Fröhlich) and the US NASA's ACRIM team (Dr. Richard C. Willson). This work is supported by the Canadian Institutes of Health Research and Natural Science and Engineering Research Council of Canada.

References

1. L. G. Christophorou, D.L. McCorkle and A. A. Christodoulides, in *Electron-Molecule Interactions and Their Applications*, Edited by L. G. Christophorou, Vol. 1 (Academic Press, Orlando, 1984), chap. 6.
2. St.-J. Dixon-Warren, E. T. Jensen and J. C. Polanyi, *Phys. Rev. Lett.* **67**, 2395 (1991).
3. W. C. Simpson and J. A. Yarmoff, *Ann. Rev. Phys. Chem.* **47**, 527 (1996).
4. R. E. Johnson, *Energetic Charge-Particles Interactions with Atmospheres and Surfaces*, Physics and Chemistry in Space Planetology, Vol. 19 (Springer-Verlag, Berlin, 1990).
5. R. A. Marcus, *Rev. Mod. Phys.* **65**, 599 (1993) (Nobel Lecture).
6. C. Wan, T. Fiebig, O. Schiemann, J. K. Barton and A. H. Zewail, *Proc. Natl. Acad. Sci. USA.* **97**, 14052 (2000).
7. Q.-B. Lu, *Phys. Rep.* **487**, 141 (2010).

8. Q.-B. Lu, *Mutat. Res.: Rev. Mutat. Res.* **704**, 190 (2010).
9. Q.-B. Lu and T. E. Madey, *J. Chem. Phys.* **111**, 2861 (1999).
10. Q.-B. Lu and T. E. Madey, *Phys. Rev. Lett.* **82**, 4122 (1999).
11. Q.-B. Lu and L. Sanche, *Phys. Rev. Lett.* **87**, 078501 (2001).
12. Q.-B. Lu, *Phys. Rev. Lett.* **102**, 118501 (2009).
13. C.-R. Wang, J. Nguyen and Q.-B. Lu, *J. Am. Chem. Soc.* **131**, 11320 (2009).
14. J. Nguyen, Y. Ma, T. Luo, R. G. Bristow, D. A. Jaffray, Q.-B. Lu, *Proc. Natl. Acad. Sci. USA* **108**, 11778 (2011).
15. Q.-B. Lu and T. E. Madey, *Surf. Sci.* **451**, 238 (2000).
16. Q.-B. Lu and T. E. Madey, *J. Phys. Chem. B* **105**, 2779 (2001).
17. S. Solovev, D. O. Kusmirek and T. E. Madey, *J. Chem. Phys.* **120**, 968 (2004).
18. Q.-B. Lu and L. Sanche, *Phys. Rev. B* **63**, 153403 (2001).
19. Q.-B. Lu and L. Sanche, *J. Chem. Phys.* **115**, 5711 (2001).
20. Q.-B. Lu and L. Sanche, *J. Chem. Phys.* **120**, 2434 (2004).
21. S. Ryu, J. Chang, H. Kwon and S. K. Kim, *J. Am. Chem. Soc.* **128**, 3500 (2006).
22. Y. Sohn, W. Wei and J. M. White, *Surf. Sci.* **602**, 2706 (2008).
23. H. Tachikawa, *Phys. Chem. Chem. Phys.* **10**, 2200 (2008).
24. M. Bertin, M. Meyer, J. Stähler, C. Gahl, M. Wolf and U. Bovensiepen, *Faraday Discuss.* **141**, 293 (2009).
25. S. K. Bhattacharya, J. M. Finn, V. P. Diep, F. Baletto and S. Scandolo, *Phys. Chem. Chem. Phys.* **12**, 13034 (2010).
26. J. Stähler, C. Gahl and M. Wolf, *Acc. Chem. Res.* **45**, 131 (2012).
27. I. I. Fabrikant, S. Caprasecca, G. A. Gallup and J. D. Gorfinkiel, *J. Chem. Phys.* **136**, 184301 (2012).
28. C.-R. Wang, A. Hu and Q.-B. Lu, *J. Chem. Phys.* **124**, 241102 (2006).
29. C.-R. Wang and Q.-B. Lu, *Angew. Chem. Intl. Ed.* **46**, 6316 (2007).
30. Q.-B. Lu, *J. Med. Chem.* **50**, 2601 (2007).
31. Q.-B. Lu, S. Kalantari and C.-R. Wang, *Mol. Pharmaceutics* **4**, 624 (2007).
32. C.-R. Wang, K. Drew, T. Luo, M.-J. Lu and Q.-B. Lu, *J. Chem. Phys.* **128**, 041102 (2008).
33. C. R. Wang, T. Luo and Q.-B. Lu, *Phys. Chem. Chem. Phys.* **10**, 4463 (2008).
34. C.-R. Wang and Q.-B. Lu, *J. Am. Chem. Soc.* **132**, 14710 (2010).
35. Q.-B. Lu, *J. Cosmology* **8**, 1846 (2010).
36. J. V. Revadekar and S. D. Patil, *Atmos. Environ.* **45**, 6658 (2011).

37. P. J. Crutzen, S. A. Isaksen and G. C. Reid, *Science* **189**, 457(1975).
38. M. A. Ruderman, H. M. Foley and J. W. Chamberlain, *Science* **192**, 555 (1976).
39. R. M. Thorne, *Science* **195**, 287 (1977).
40. C. H. Jackman, *J. Geomagnet. Geoelectri.* **43**, S637-646 (1991).
41. A. A. Krivolutsky, *Adv. Space Res.* **27**, 1993-2002 (2001).
42. N. Gehrels, C. M. Laird, C. H. Jackman, J. K. Cannizzo, B. J. Mattson and W. Chen, *Astrophys. J.* **585**, 1169-1176 (2003).
43. B. C. Thomas, C. H. Jackman, A. L. Melott, C. M. Laird, R. S. Stolarski, N. Gehrels, J. K. Cannizzo and D. P. Hogan, *Astrophys. J.* **622**, L153-L156 (2005).
44. A. L. Melott, A. J. Krejci, B. C. Thomas, M. V. Medvedev, G. W. Wilson and M. J. Murray, *J. Geophys. Res.* **113**, E10007 (2008).
45. B. Jan and M. A. K. Y. Zai, *J. Basic & Applied Sci.* **8**, 370-373 (2012).
46. C. R. Beckie, *Determining the Polar Cosmic Ray Effect on Cloud Microphysics and the Earth's Ozone Layer*, UCGE Reports No. 20356 (The University of Calgary, 2012).
47. J. A. Eddy, *Science* **192**, 1189 (1976).
48. G. C. Reid, *Nature* **329**, 142 (1987).
49. E. Friis-Christensen and K. Lassen, *Science* **254**, 698 (1991).
50. D. V. Hoyt and K. H. Schatten, *J. Geophys. Res.* **98**, 18895 (1993).
51. J. Lean, J. Beer and R. Bradley, *Geophys. Res. Lett.* **22**, 3195 (1995).
52. R. C. Willson, *Science* **277**, 1963 (1997).
53. S. K. Solanki and M. Fligge, *Geophys. Res. Lett.* **25**, 341 (1998).
54. S. K. Solanki and N. A. Krivova, *J. Geophys. Res.* **108**, 1200 (2003).
55. P. Foukal, C. Fröhlich, H. Spruit and T. M. L. Wigley, *Nature* **443**, 161 (2006).
56. C. Fröhlich, *Space Sci. Rev.* **125**, 53 (2006).
57. M. Lockwood and C. Fröhlich, *Proc. R. Soc. A* **463**, 2447 (2007).
58. H. Svensmark and E. Friis-Christensen, *J. Atmos. Sol. Terr. Phys.* **59**, 1225 (1997).
59. F. Q. Yu, and R. P. Turco, *J. Geophys. Res.* **106**, 4797 (2001).
60. J. Kirkby et al., *Nature* **476**, 429 (2011).
61. F. Yu, *Atmos. Chem. Phys.* **4**, 1037 (2004).
62. E. A. Kasatkina and O. I. Shumilov, *Annal. Geophys.* **23**, 675 (2005).
63. M. J. Molina and F. S. Rowland, *Nature* **249**, 810-812 (1974).
64. O. B. Toon and R. P. Turco, *Sci. Ameri.* **264**, 68-74 (1991).

65. World Meteorological Organization (WMO), *Scientific Assessment of Ozone Depletion: 1994* (Global Ozone Research and Monitoring Project-Report No. 47, Geneva, 1995).
66. World Meteorological Organization (WMO), *Scientific Assessment of Ozone Depletion: 2006* (Global Ozone Research and Monitoring Project-Report No. 50, Geneva, 2007).
67. World Meteorological Organization (WMO), *Scientific Assessment of Ozone Depletion: 2010* (Global Ozone Research and Monitoring Project-Report No. 52, Geneva, 2011).
68. J. C. Farman, B.G. Gardiner and J. D. Shanklin, *Nature* **315**, 207-210 (1985).
69. G. L. Manney et al., *Nature* **478**, 469 (2011).
70. W. M. Hickam and D. Berg, *J. Chem. Phys.* **29**, 517 (1958).
71. R. K. Curran, *J. Chem. Phys.* **34**, 2007 (1961).
72. J. P. Johnson, L. G. Christophorou and J. G. Carter, *J. Chem. Phys.* **67**, 2196 (1977).
73. E. Illenberger, H.-U. Scheunemann and H. Baumgärtel, *Chem. Phys.* **37**, 21 (1979).
74. S. D. Peyerimhoff and R. J. Buenker, *Chem. Phys. Lett.* **65**, 434 (1979).
75. M. Lewerenz, B. Nestmann, P. J. Bruna and S. D. Peyerimhoff, *J. Mol. Structure (Theochem)* **123**, 329 (1985).
76. D. Smith and N. G. Adams, *Top. Curr. Chem.* **89**, 1 (1980).
77. D. G. Torr, in *The Photochemistry of Atmospheres*, Edited by J. S. Levine, (Academic Press, Orlando, 1985), chap. 5.
78. V. Ramanathan, *Science* **190**, 50 (1975).
79. V. Ramanathan, L. Callis, R. Cess, J. Hansen, I. Isaksen, W. Kuhn, A. Lacis, F. Luther, J. Mahlamn, R. Reck and M. Schlesinger, *Rev. Geophys.* **25**, 1441 (1987).
80. W. C. Wang and G. Molnar, *J. Geophys. Res.* **90**, 12971 (1985).
81. W. C. Wang et al., *Nature* **350**, 573 (1991).
82. P. M. De F. Forster and M. Joshi, *Climate Change* **71**, 249 (2005).
83. IPCC Report, Third Assessment Report: Climate Change (TAR) (2001).
84. IPCC Report, Fourth Assessment Report: Climate Change (AR4) (2007).
85. Q.-B. Lu, [arXiv:1210.1498](https://arxiv.org/abs/1210.1498) (2012).
86. J. G. Anderson, J. A. Dykema, R. M. Goody, H. Hua and D. B. Kirk-Davidoff, *J. Quant. Spectrosc. & Radiat. Transfer* **85**, 367 (2004).
87. H. Fischer, M. Wahlen, J. Smith, D. Mastroianni and B. Deck, *Science* **283**, 1712 (1999).
88. N. A. Krivova, S. K. Solanki, T. Wenzler and B. Podlipnik, *J. Geophys. Res.* **114**, D00I04 (2009).
89. C. Fröhlich, *Space Sci. Rev.* (2011), DOI 10.1007/s11214-011-9780-1.
90. S. K. Solanki and N. A. Krivova, *Science* **334**, 916 (2011).

Data Sets (Sources). NASA TOMS (N7/M3/EP) and OMI ozone satellite datasets were obtained from <http://toms.gsfc.nasa.gov>. The CH₄ and CF₂Cl₂ data in the stratosphere were obtained from the NASA Goddard Space Flight Center (GDSC) CLAES datasets. The O₃ and lower stratospheric temperature data at Rothera and Halley, Antarctica were from the British Antarctic Survey (BAS) (<http://www.antarctica.ac.uk/met/jds/ozone/>), credited to Dr. Jon D. Shanklin. Near Real Time satellite data of CFC-12, N₂O and CH₄ were from The University of Oxford's MIPAS team (Dr. Anu Dudhia) (<http://www.atm.ox.ac.uk/group/mipas/L2OXF/trend/>). Cosmic ray data at McMurdo were from the Neutron monitors of the Bartol Research Institute <http://neutronm.bartol.udel.edu>). Cosmic ray data for other detecting stations were from the Network of Cosmic Ray Stations (<http://cr0.izmiran.rssi.ru/common/links.htm>). The sunspot number data were from the Royal Observatory of Belgium's Solar Influences Data Analysis Center (<http://sidc.oma.be/>). The PMOD TSI data were from the Swiss Science Foundation's PMOD / WRC team (Dr. Claus Fröhlich) (<http://www.pmodwrc.ch/pmod.php?topic=tsi/composite/SolarConstant>), while the ACRIM TSI data were from the US NASA's ACRIM team (Dr. Richard C. Willson) (<http://www.acrim.com/>). Global surface temperature data were from two sources, namely the UK Met Office Hadley Centre: the HadCRUT3 dataset, combined land-surface air temperature and sea-surface temperature anomalies (<http://hadobs.metoffice.com/>), and the US NOAA National Climatic Data Center (NCDC): the dataset of annual global (combined land and ocean temperature) anomalies (<http://www.ncdc.noaa.gov/oa/climate/research/anomalies/index.html>). CO₂ data from 1850 to 1958 were from the US DOE Oak Ridge National Laboratory (ORNL)'s Carbon Dioxide Information Analysis Center (CDIAC)'s Law Dome DE08, DE08-2, and DSS ice core measurements (<http://cdiac.ornl.gov/trends/co2/lawdome-data.html>); for the years without recorded data, a linear extrapolation was used to obtain the CO₂ data between two closest recorded data points. CO₂ data after 1958 were from direct atmospheric measurements at Mauna Loa Observatory, Hawaii by the NOAA's Global Monitoring Division (GMD) (<http://www.esrl.noaa.gov/gmd/ccgg/trends/>). Halocarbon concentrations and EECI values were from the WMO Reports^{66,67} or from the NOAA's GMD.